Technische Universität München

TUM School of Life Sciences

Lehrstuhl für Molekulare Ernährungsmedizin

The role of SULT1A1 in whole body metabolism and adipocyte biology

Margherita Springer

Vollständiger Abdruck der von der TUM School of Life Sciences der Technischen Universität München zur Erlangung des Grades eines

Doktors der Naturwissenschaften

genehmigten Dissertation.

Vorsitzender:	apl. Prof. Dr. Kurt Gedrich
Prüfer der Dissertation:	1. Prof. Dr. Martin Klingenspor
	2. Prof. Dr. Hubert Vidal

Die Dissertation wurde am 12.11.2020 bei der Technischen Universität München eingereicht und durch die TUM School of Life Sciences am 26.02.2021 angenommen.

Table of Contents

List of figures and tables

Figures

Tables

List of supplementary figures and tables

Supplementary figures

Supplementary tables

Abbreviations

ANCOVA	analysis of covariance
ATP	adenosine triphosphate
BAT	brown adipose tissue
BMI	body mass index
ChREBP	carbohydrate-responsive element-binding protein
CO2	carbon dioxide
cpm	counts per minute
cRCR	cellular respiratory control ratio
CT	constitutional thinness
DNL	de novo lipogenesis
ECM	extracellular matrix
EE	energy expenditure
eWAT	epididymal white adipose tissue
FCCP	carbonyl cyanide-4-(trifluoromethoxy)phenylhydrazone
FGF21	fibroblast growth factor 21
H&E	hematoxylin and eosin
HFD	high-fat diet
IP	intraperitoneal
IPA	Ingenuity Pathway Analysis
IPGTT	intraperitoneal glucose tolerance test
IPITT	intraperitoneal insulin tolerance test
iWAT	inguinal white adipose tissue
KO	knockout
LBP	liposaccharide binding protein
LPS	lipopolysaccharides
LXR	liver X receptor
NAFLD	non-alcoholic fatty liver disease
O2	oxygen
p-NP	p-nitrophenol
PAP	3'-phosphoadenosine-5'-phosphate
PAPS	3'-phosphoadenosine-5'-phosphosulfate
qNMR	quantitative Nuclear Magnetic Resonance
rWAT	retroperitoneal white adipose
SD	standard deviation
SEM	standard error of the mean
SGBS	Simpson-Golabi-Behmel syndrome
SR	Sirius red

SREBP1	sterol regulatory element-binding protein 1
SULT1A1	sulfotransferase 1A1
SVF	stromal vascular fraction
TEE	total energy expenditure
TG	triglycerides
UCP1	uncoupling protein 1
UGT	uridine 5′-diphospho-glucuronosyltransferases
UHPLC-UV	ultra-high performance liquid chromatography-ultraviolet
VDAC	voltage-dependent anion-selective channel 1
WT	wild-type

Abstract

Constitutional thinness (CT) is a unique phenotype of human leanness and resistance to weight gain. CT individuals have a normal body fat percentage but low body weight [body mass index (BMI) < 18 kg/m^2]. These individuals express a desire to gain weight but cannot despite consuming excess food. To gain insight into the CT phenotype, a previous experiment compared the adipose tissue of the constitutionally thin to normal body weight controls. Transcriptomics and subsequent differential gene expression analysis indicated that sulfotransferase 1A1 (SULT1A1) was the most downregulated transcript in the adipose tissue of CT subjects. SULT1A1 codes for an enzyme called sulfotransferase 1A1 which catalyzes the transfer of sulfur to endogenous and exogenous substrates within the body with no known function in adipose tissue. To determine if SULT1A1 contributes to the constitutionally thin phenotype a mouse model was used as SULT1A1 tissue expression is similar between humans and mice. To model reduced SULT1A1 expression a whole-body Sult1a1 knockout (KO) mouse strain was studied. Sult1a1 KO mice have a low body weight and are resistant to weight gain on a high-fat diet (HFD) mirroring characteristics of the CT phenotype. Adipose tissue from CT individuals and Sult1a1 KO mice show a shift from energy storage to energy dissipating pathways with differences in the molecular mechanism driving the phenotype. Subcutaneous adipose tissue from Sult1a1 KO mice has elevated leak respiration, uncoupling protein 1 (UCP1) expression and increased mitochondrial content indicating that Sult1a1 plays a role in adipose tissue browning. Sult1a1 KO mice recapitulate features of the CT phenotype linking SULT1A1 to human leanness.

Zusammenfassung

Konstitutionelle Schlankheit [Constitutional thinness (CT)] ist ein seltener Phänotyp menschlicher Magerkeit, der sich durch eine Resistenz gegen Gewichtszunahme auszeichnet. CT-Menschen haben trotz normalem Körperfettanteil ein sehr geringes Körpergewicht [Body Mass Index (BMI) < 18 kg/m^2]. CT-Personen äußern den Wunsch, an Gewicht zuzunehmen, können dies jedoch trotz überschüssiger Energiezufuhr nicht erreichen. Um den CT-Phänotyp besser zu verstehen, wurde in einer vorhergehenden Studie das Fettgewebe von CT-Personen mit dem Normalgewichtiger verglichen. Transkriptomik und anschließende differentielle Genexpressionsanalysen zeigten, dass Sulfotransferase 1A1 (SULT1A1) das am stärksten herunterregulierte Transkript im Fettgewebe der CT-Probanden ist. Das Genprodukt von SULT1A1, das Enzym Sulfotransferase 1A1 (SULT1A1), katalysiert den Transfer von Schwefel auf endogene und exogene Substrate im Körper. Eine spezifische Funktion von SULT1A1 im Fettgewebe war bisher jedoch nicht bekannt. Im Körper ähnelt sich die SULT1A1-Gewebeexpression von Menschen und Mäusen. Im Ganzkörper-Sult1a1-Knockout (KO)-Mausmodell sollte darum geklärt werden, ob die beobachtete reduzierte SULT1A1-Expression zum menschlichen CT-Phänotyp beiträgt. Ähnlich dem CT-Phänotyp im Menschen besitzen Sult1a1 KO-Mäuse ein niedriges Körpergewicht und sind resistent gegen eine Gewichtszunahme unter fettreicher Diät. Obgleich sich die zugrundeliegenden molekularen Mechanismen zwischen Mensch und Maus unterscheiden, zeigt sich, dass in beiden Organismen eine Verschiebung von Energiespeicher- zu Energiedissipationswegen stattfindet und den CT-Phänotyp antreibt. Subkutanes Fettgewebe von Sult1a1 KO-Mäusen weist ein erhöhtes Proton-Leck, eine gesteigerte Expression von Uncoupling Protein 1 (UCP1) und einen höheren Mitochondriengehalt auf. Diese Ergebnisse deuten darauf hin, dass Sult1a1 in Mäusen eine Rolle bei der Bräunung von Fettgewebe spielt. Das Sult1a1-KO-Mausmodell rekapituliert somit Merkmale des menschlichen CT-Phänotyps und bringt SULT1A1 mit der menschlichen Schlankheit in Verbindung.

1. Introduction

Obesity is a public health issue that raises healthcare costs, decreases quality of life and increases the risk of developing a chronic illness like type 2 diabetes, cardiovascular disease and cancer (1). A key feature of obesity is the accumulation of body fat that occurs when there is a long term imbalance between energy intake and energy expenditure (EE) (1). BMI is positively correlated with body fat stores (2) and disease risk (3). Adults can be classified as underweight (BMI < 18.5), normal weight (BMI = 18.5-24.9), overweight (BMI = 25-29.9) or obese (BMI ≥ 30) according to their BMI. In 2016, the World Health Organization estimated that 650 million adults were obese which represented 13% of the worldwide population (4). The prevalence of obesity is projected to double by 2030 (5). Reducing obesity prevalence would improve quality of life for a large share of the population. Obesity is a complex disorder caused by both genetic and environmental factors (1). Studies of obesity have mainly focused on overweight and obese individuals however a subset of studies are beginning to investigate leanness and weight gain resistance to understand the factors underlying low BMI maintenance (6–9). Studies of lean and weight gain resistant individuals may complement our understanding of obesity by identifying factors that promote leanness and prevent weight gain.

CT is a unique phenotype of human leanness and resistance to weight gain. CT individuals have a body composition within the normal range but low body weight [BMI < 18 kg/m^2] and express a strong desire to gain weight (10). To understand the CT phenotype, the adipose tissue transcriptome from the constitutionally thin and normal weight controls was compared since adipose tissue is a key regulator of body weight (11). The most downregulated transcript in the adipose tissue of the constitutionally thin was SULT1A1 (**Fig. 1**). The SULT1A1 transcript codes for a protein which catalyzes the transfer of sulfonate groups (12). A recent clinical trial described differences in the morphology and function of adipose tissue from the constitutionally thin which has reduced adipocyte size and greater mitochondrial respiratory capacity accompanied by increased mitochondrial content. Pathway analysis of differentially expressed genes identified an enrichment of genes annotating to lipid metabolism and inhibition of proinflammatory signaling pathways in CT adipose tissue (7). Additionally, genome wide association studies have linked

susceptibility loci mapping close to SULT1A1 with BMI (8,13). Together this evidence suggests a role for SULT1A1 in adipose tissue function and energy metabolism.

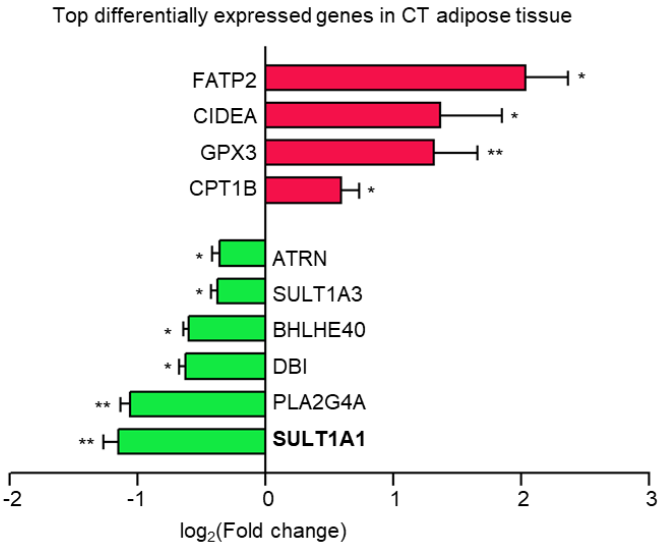

Fig. 1: Reduced expression of SULT1A1 in the adipose tissue of the constitutionally thin. Adipose tissue was collected from eight CT women and eight age-matched normal weight controls. mRNA expression was measured using a microarray and then confirmed by qPCR. Data presented as $\log_2$ fold change (CT/control) of qPCR validation data, error bar represents standard deviation (SD) of ratio, p-value calculated using Student t test, *p ≤ 0.05 and ** p ≤ 0.01.

Previous to this thesis, SULT1A1 was uncharacterized in adipose tissue and not yet linked to energy metabolism. SULT1A1 has been studied in the liver, kidney and the gastrointestinal tract for its function as a sulfotransferase. SULT1A1 belongs to a large group of related enzymes which catalyze the transfer of sulfonate to endogenous and exogenous substrates. The transfer of sulfonate requires a co-factor called 3'-phosphoadenosine-5'-phosphosulfate (PAPS) which is the endogenous source of sulfur for the sulfotransferases. Together PAPS and SULT coordinate a process called sulfate conjugation which results in the release of 3'-phosphoadenosine-5'-phosphate (PAP) and a sulfonated substrate. Sulfate conjugation, and conjugation reactions in general, have been associated with detoxification as sulfate conjugation lowers the biological activity of molecules and increases their water solubility facilitating excretion (12). However, sulfate conjugation can also bioactivate molecules, typically ones found in processed foods, generating chemical species which can covalently bind to DNA and promote carcinogenesis (14–16).

The human genome encodes 13 SULT genes (12,17,18). There are four families of sulfotransferases in humans: SULT1, SULT2, SULT4 and SULT6 (18,19). The SULT1 and SULT2 families have been characterized while the SULT4 and SULT6 families have been identified but their function in humans is still unclear. SULT1A1 belongs to the SULT1 family which also contains SULT1A2, SULT1A3, SULT1A4, SULT1C2, SULT1C3, SULT1C4 and SULT1E1. The SULT1 family share high amino acid sequence similarity. Within the SULT1 family the PAPS binding domain and that catalytic residues are conserved. However, the substrate binding site shows variation explaining differences in substrate affinities. For example, SULT1A1 and SULT1A2 share high sequence similarity and have similar substrates, however due to differences in the substrate binding site, SULT1A2 has much lower affinity for SULT1A1 substrates (18).

SULT1A3 has only been identified in humans because through selection they have evolved to develop a specific sulfotransferase for the sulfonating of catecholamines like dopamine (20) and norepinephrine (12). SULT1A3 is sometimes referred to as SULT1A3/4 because there are two copies of this gene present on chromosome 16 with both genes transcriptionally active (21). SULT1A3 was amongst the most downregulated genes in the adipose tissue of the constitutionally thin (**Fig. 1**). In humans, there are no known endogenous substrates for the SULT1C family. The SULT1C family has affinity towards simple phenolic substrates like p-nitrophenol (p-NP). The main substrate for SULT1E1 are endogenous and synthetic estrogens and thyroid hormone. SULT1A1 and 1A2 have some affinity towards estrogen but only at concentrations that are outside the physiological range (12).

The SULT2 family contains SULT2A1, SULT2B1_v1 and SULT2B1_v2 these enzymes sulfonate steroids and are known as the hydroxysteroid sulfotransferases (12). Members of the SULT2 family also have affinity towards exogenous substrates. SULT4 and SULT6 are the least characterized families and both contain a single SULT enzyme. The SULT4 family contains SULT4A1, which has no known substrate. SULT4A1 may lack the ability to catalyze the transfer of sulfonate as it does not contain a binding site for PAPS. Though SULT4A1 lacks a substrate and a PAPS binding site, the SULT4A1 sequence is highly conserved among species indicating that SULT4A1 may have an important function (18). The SULT6 family contains a single enzyme, SULT6B1, which has no known substrate in humans (18) though in mice Sult6b1 has affinity towards endogenous and exogenous substrates (22).

A typical substrate for SULT1A1 are exogenous compounds that contain a phenolic ring like resveratrol, a molecule synthesized in grape skin (23). Commercially available resveratrol is extracted from Japanese knotweed which is an abundant source of resveratrol (24). Resveratrol binds directly to molecules involved in energy metabolism, inflammatory signaling, cell cycle regulation and post translational modifications which has linked resveratrol to protection against diet induced obesity, improved longevity and cancer prevention (25). When ingested, resveratrol is metabolized to resveratrol-sulfate and resveratrol-glucuronide, via SULTs and uridine 5′-diphospho-glucuronosyltransferases (UGT), respectively. Resveratrol and its microbial metabolites, hydroxy-resveratrol, which have similar biological activity can be sulfonated and have a greatly reduced biological activity (26). Biochemical studies have shown that SULT1A1 is the main SULT responsible for the sulfation of resveratrol into resveratrol-3-*O*-sulfate, which is the main sulfonated metabolite produced in humans (27). Reduced bioavailability of resveratrol through conjugation reactions represents one of the major challenges of translating cellular observations to pre-clinical and clinical studies and there is an interest in improving the bioavailability of resveratrol and other bio-active phenolic compounds.

In humans, SULT1A1 is located on chromosome 16 (12) and contains 6 exons (28). SULT1A1 is abundantly expressed in the lungs, liver, gastrointestinal tract and kidney (29). Investigation of the CT phenotype demonstrated expression of SULT1A1 in adipose tissue, an observation confirmed from data retrieved from the BioGPS database (30). In the mouse, a model organism used in this thesis, Sult1a1 is located on chromosome 7 and contains 7 exons (31). The substrate binding domain of human SULT1A1 occurs at amino acid position 106 – 108 (32) and is conserved within mice (33). Like humans, mice express Sult1a1 in the adipose tissue (34), lungs, liver, kidney and gastrointestinal tract (35). Humans express SULT1A1 in the small intestine (30) while mice express Sult1a1 in the colon (35). To investigate the role of SULT1A1 in adipose tissue function and energy metabolism, a mouse model was used as tissue distribution of SULT1A1 is similar between mice and humans. A whole-body Sult1a1 KO mouse was characterized on a purified standard diet and a HFD.

Adipose tissue is a key regulator of energy balance and alterations to adipose tissue homeostasis impacts whole body metabolism. Adipose tissue is located within the body in distinct depots either subcutaneously or viscerally (36). Depots can be further divided by anatomical proximity to other organs for example epididymal white adipose tissue (eWAT) is a visceral depot that surrounds the gonads and retroperitoneal white adipose (rWAT) is a visceral depot that surrounds the kidneys. Adipose tissue is mainly composed of adipocytes but also contains many other cell types like immune cells, fibroblasts, endothelial cells and pre-adipocytes. To date three different types of adipocytes have been described: white, brown and beige which are differentiated from each other based on UCP1 expression and anatomical location (36,37). White adipocytes do not express significant amounts of UCP1 while brown adipocytes express high levels of UCP1. Beige adipocytes are typically located in white adipose tissue depots but show higher UCP1 expression. For this reason beige adipocytes are also referred to as brite (brown in white) adipocytes. UCP1, is a protein located on the inner mitochondrial membrane and uncouples the electron transport chain from adenosine triphosphate (ATP) production by allowing protons that are pumped into the outer mitochondrial matrix to re-enter the inner mitochondrial membrane bypassing ATP synthase (38). Adipose tissue functions as an energy storage depot, an endocrine tissue and produces heat through non-shivering thermogenesis (37) depending on the anatomical site and adipocyte type.

In obesity, there are dramatic changes to the adipose tissue. There are changes in the number (hyperplasia) and size of the adipocytes (hypertrophy). The propensity towards hyperplasia and hypertrophy depend on depot and gender. As the adipocyte expands, the extracellular matrix (ECM) expands to maintain the integrity of the adipocyte. Excessive ECM deposition, infiltration of macrophages, reduced mitochondrial function and altered adipokine and lipid profiles are hallmarks of adipose tissue dysfunction in obesity (39). On the whole body level, as adipose tissue depots expand, serum triglycerides (TG) increase and lipids accumulation ectopically within the liver and skeletal muscle which impairs insulin signaling and promotes insulin resistance.

Thesis objectives

Since SULT1A1 expression was reduced in the adipose of the constitutionally thin and there is no known role for SULT1A1 in adipose tissue this thesis aims to determine if SULT1A1 contributes to the constitutionally thin phenotype. To investigate the role of SULT1A1 in adipose tissue function and energy metabolism, a mouse model was used as tissue distribution of SULT1A1 is similar between mice and humans. A whole-body Sult1a1 KO mouse was characterized on a purified standard diet and a HFD. The HFD intervention was included to evaluate if deletion of Sult1a1 protected mice from the harmful effects of diet induced obesity namely hyperglycemia, insulin resistance, inflammation and ectopic lipid accumulation. The metabolic phenotype of the Sult1a1 KO strain was evaluated with a pipeline of interventions designed to detect differences in body weight and composition, EE and glycemia. A subset of mice from the standard purified diet were further analyzed for characterization of adipose tissue respiratory capacity. To validate the Sult1a1 KO mouse model, Sult1a1 KO mice were treated with a SULT1A1 substrate and tissue concentration was quantified using ultra-high performance liquid chromatography-ultraviolet (UHPLC-UV) detection.

2. Materials and Methods

Phenotyping of Sult1a1 KO mice received ethical approval from the animal studies committee at the Nestlé Institute of Health Science and the French Ministry of Research under authorization number 18574. All animal experiments were performed in compliance with the European Community regulation for laboratory animal care and use (Directive 2010/63/UE).

Rederivation of the Sult1a1 mouse colony

To generate the Sult1a1 knockout mice, mature oocytes from female mice were fertilized from the sperm of three, 24 week old Sult1a1 KO mice in vitro. The male Sult1a1 KO mice were provided by the German Institute for Human Nutrition and developed as described in a previous publication (40). In Sult1a1 mutant mice, exons 2 to 4 are replaced by a neomycin cassette (**Supplementary Fig. 1**). Fertilized oocytes were transferred to 30 recipient females to generate mice heterozygous for the Sult1a1 KO gene. Breeding cages were established by pairing six week old, heterozygous male and female mice in duos. The offspring were

genotyped by PCR using primers amplifying a 397 bp region of Sult1a1 DNA and a 171 bp region of the neomycin cassette (**Supplementary Table 1**). Six week old offspring from homozygous breeding pairs were phenotyped with a pipeline of interventions designed to detect differences in body weight and composition, EE and glycemia (**Table 1**). Adipose tissue respiratory capacity was characterized for a subset of mice on the standard diet.

Table 1: Pipeline for metabolic phenotyping of the Sult1a1 KO mouse strain.

Age (weeks)	Intervention/Action
6	Randomize mice into experimental groups
7	Switch from house chow to standard purified diet or high fat diet
14	Measure body composition Indirect calorimetry
16	Fast mice overnight in preparation for glucose tolerance test Collect blood for blood glucose measurement and insulin measurement
18	Fast mice (morning fast) in preparation for insulin tolerance test Collect blood for blood glucose measurement
20	Measure body composition Fast mice overnight for blood collection Biological sample collection (eWAT, rWAT, liver, skeletal muscle and colon)
24	Assessment of adipose tissue mitochondrial respiration capacity

Metabolic phenotyping of Sult1a1 KO mice

Sult1a1 KO and wild-type (WT) mice had *ad libitum* access to food and water and maintained on a 12 hour light/dark cycle at a temperature between 20-24°C and a relative humidity between 50-60%. At six-weeks old, male mice were removed from their home cages and allocated either a standard purified diet (standard diet) or a HFD group. Mice from the same litter were kept together in the new experimental cage with 2-4 mice per cage. For some cages, litters were separated when there were more than 4 pups. At seven-weeks old, the diet was switched from the standard rodent chow diet (D04, Safe) to either a HFD (D12451i, Research Diets) with 45% kcal from fat or a standard purified diet (D12450H, Research Diets) with 10% kcal from fat for 14 weeks with a sample size of 15 mice per group. Caretakers completed a weekly welfare scoresheet for each mouse to monitor health status. Body weight was recorded at the same time each week.

Indirect calorimetry

Oxygen (O_2) consumption, carbon dioxide (CO_2) production, activity and food intake were measured using the LabMaster system (LabMaster, TSE Systems). Mice aged 14-weeks old were individually housed in the LabMaster system cages for 48 hours under a 12h light/12h dark photoperiod at ambient temperature (21°C ± 2). Data analysis was performed on recordings following a 24h-acclimatization period. The analysis included 24 hours which included part of the light period of the first day of recording, followed by one complete dark period and part of the light period of the second day of recording (i.e. 12:00 pm Day 1 to 11:00am Day 2). EE was calculated with an average of the VO_2 and VCO_2 hourly-recording using the formula, EE (J) = 15.818(VO_2) + 5.176(CO_2) previously described (41). To adjust EE for differences in lean mass, body composition was measured after indirect calorimetry. Total lean and fat weight were measured using quantitative Nuclear Magnetic Resonance (qNMR) (Minispec, Bruker) during the light period on conscious fed mice. Body composition was measured a second time using qNMR on 20-week old mice.

Respirometry of adipocytes

Isolation and preparation of adipocytes

Oxygen consumption of adipocytes was measured according to previously established methods (42,43). Oxygen consumption was measured from adipocytes isolated from inguinal white adipose tissue (iWAT) and eWAT of WT (n = 6) and Sult1a1 KO (n = 4) mice on a standard diet. Mice were exposed to carbon CO_2 with flow set to 1.7 L/minute. Adipose tissue depots were dissected immediately after death and manually minced in 5 ml of isolation medium in a 15 ml Falcon tube. After mincing, the tube was topped up to 7 ml with isolation medium and then shaken (Cat # WIS-20, WiseCube) at 150 rpm and 37ºC for 20 minutes. The isolation medium contained Collagenase B (Cat # 11088815001, Sigma) at 1g/L in Hank's Balanced Salt Solution (Cat # 14025050, Thermo Fisher) which contained 4% BSA. After checking that the adipose tissue samples were digested the samples were filtered with 250 µm mesh into a new 15 ml falcon tube. After filtering, the samples were centrifuged for 2 minutes at 300g which separates the samples into three fractions, a top fatty layer, which contains the adipocytes measured, a middle liquid fraction and at the bottom a pellet containing the stromal vascular fraction (SVF). A long syringe needle was used to remove the middle fraction and the remaining adipocytes were washed with 10 ml of BSA and then

centrifuged for 2 minutes at 300g. Washing and centrifugation was repeated a second time followed by a final wash with 10 ml of BSA fatty acid free. BSA and BSA fatty acid free solutions contained 2 g of either BSA and BSA fatty acid free in STE buffer which contained 250 mM sucrose (Carl Roth), 5 mM Tris (Carl Roth), 2 mM EGTA (Carl Roth), pH = 7.4 at 4°C. A pipette with the tip cut off was used to collect the fatty layer and then hung off the edge of the bench to fully separate the liquid BSA fraction from the fat. The BSA fraction was discarded and remaining fatty layer was transferred to a clean Eppendorf and then kept on ice until measurement.

High-resolution respirometry using Oroboros

To prepare the Oroboros chambers for measurement, the ethanol contained in the chambers was aspirated and then the chamber was washed 5 times with water making sure to also flush the plugs. Stirring was disactivated and 2.2 ml of MIR05 buffer was added to the chamber and left of oxygenate for 15 minutes. The MIR05 buffer contained 110 mM sucrose, 60 mM potassium lactobionate, 0.5 mM EGTA, 3 mM $MgCl_2$*$6H_2O$, 20 mM taurine, 10 mM KH_2PO_4, 20 mM Hepes, 1 g/L BSA-fatty acid free and 5 mM malate, pH 7.1 at 37°C. After buffer oxygenation, ≈ 100 µl isolated adipocytes were added to the chamber. Substrates and inhibitors were injected into the chamber at the concentrations described in **Table 2** and oxygen consumption was measured. After measurement, the contents of the chamber were collected to quantify DNA concentration. Before starting a new measurement, the chamber was washed with 100% ethanol for no more than 15 minutes and then washed 5 times with demineralized water.

Table 2: Compounds used to investigate respiratory capacity of adipocytes

Compound	Stock	Volume (µl)	Final Concentration	Function
Pyruvate	1 mM	10	5 µM	Complex I substrates
Malate	1 mM	10	5 µM	
Oligomycin	2 mg/ml	2	2 µg/ml	Complex V inhibitor
FCCP	1 mM	1	Titration dependent[#]	Uncouples electron transport from phosphorylation of ATP
Antimycin A	2.5 mM	2	2.5 µM	Complex III inhibitor

[#]Carbonyl cyanide-4-(trifluoromethoxy)phenylhydrazone (FCCP) titrated in 0.5 µM steps to achieve maximal respiration. For reference 5 injections were necessary (final concentration = 2.5 µM) to reach maximal respiration. In some cases, additional FCCP was required.

DNA quantification

DNA was isolated from 500 µl of chamber contents using the DNeasy Blood and Tissue Kit (Cat # 69504, Qiagen) according to the manufacturer's recommendations with the following modification to accommodate the larger volume of sample needed for DNA extraction. After adding ethanol (96-100%) and mixing for 30 seconds, 600 µl of mixture was added to a spin column and centrifuged for 1 minute at 8000 rpm. The follow through was discarded and then the spin column was added to a fresh tube and then the remaining volume of sample was added to the spin column and then centrifuged for 1 minute at 8000 rpm. The wash steps and elution were performed according to the protocol provided by Qiagen.

Samples were kept at -80ºC and then thawed on ice prior to DNA extraction. Samples were centrifuged each time an aliquot was taken for DNA extraction to obtain a representative sample. The samples were measured in triplicates. Genomic DNA (gDNA) was isolated to adjust the oxygen consumption data for differences in adipocyte content which varied between the measurements. To estimate DNA content, a standard curve using known DNA concentrations and Ct values was plotted. For the qPCR each well contained 5 µl master mix, 1.5 µl DNA and 3.5 µl primer mix. The master mix contained 50% qPCR grade water, 40% Light Cycler Master Mix and 10% Bright Green (Cat # 05573092001, LightCycler 1536 DNA Green Master, Roche). The Master mix was aliquoted and mixed directly with gDNA. Stock solution of primers (100 µM) were diluted to 0.9 µM. The Master mix containing gDNA and the primer mix were loaded into racks for automated pipetting (Microlab Star, Hamilton). After pipetting the plate was centrifuged for 2 minutes at 1600 rpm and then placed in a thermal cycler (Light Cycler 480 II, Roche). The primers amplified the resistin gene with the sequences described previously (42,43).

Western blot

Western blot analysis of collagenase digested adipose tissue was performed using anti-UCP1 antibodies (Cat # 14670, Cell Signaling) and anti-VDAC (Cat # 4661, Cell Signaling). Anti-vinculin (Cat # 13901, Cell Signaling) was used as a loading control. UCP1 antibody was validated with brown adipose tissue lysate (provided by Philipp Rhein) as a positive control and liver and skeletal muscle lysate as a negative control

For protein extraction, 100 µl of sucrose lysis buffer was added to 20 µl of collagenase digested adipose tissue. The sucrose lysis buffer contained 10 ml M-PER (Cat # 78501, Thermo Scientific), 250 nM sucrose (Cat # 84100, Sigma Aldrich), 1% NP-40 (Cat # 492016, Calbiochem), 1mM EDTA (Cat # AM9260G, Ambion) and 1 protease & phosphatase inhibitor tablet (Cat # A32961, Thermo Scientfic). Protein concentration was quantified using the DC Protein Assay kit according to the manufacturer's instructions (Cat # 5000116, Bio-Rad). An equal amount of sample buffer was added to each sample and incubated at 95 ºC for 5 minutes prior to gel loading. The sample buffer contained 125 mM Tris HCl (Cat # 1610799, Bio-Rad), 4% SDS (1610416, Bio-Rad), 20% glycerol (G2025, Sigma Aldrich), 0.2 M DTT (Cat # 1610611, Bio-Rad), 1% Sodium deoxycholate (Cat # 30970, Sigma Aldrich), 2% Triton-X-100 (Cat # 1610407, Bio-Rad) and 0.02% Bromophenol Blue (Cat # 1610404, Bio-Rad). A pre-cast gel (Cat # NW04127, 4-12% Bis-Tris, Invitrogen) was placed in an electrophoresis tank and 15 µg of protein lysate or 7 µl of protein standard (Cat #1610375, Bio-Rad) was added to each well. To separate the proteins, the tank was filled with running buffer (Cat # B0001, MOPS SDS Running Buffer, Bio-Rad) diluted according to the manufacturer's instructions and 100 V was applied for 2 hours. The proteins were transferred to a nitrocellulose membrane (Cat # 1704158, Bio-Rad) using a semi-dry method (Trans-Blot Tubo, Bio-Rad). The nitrocellulose membrane was blocked for 40 minutes in 5% BSA (Cat # 9998S, Cell Signaling) diluted in TBS (Cat # 1706435, Bio-Rad) with 0.05% Tween (Cat # 1706531, Bio-Rad) (TBS-T) and then incubated with the aforementioned anti-bodies overnight at 4 ºC. The dilutions used for anti-UCP1, anti-vinculin and anti-VDAC were 1:500, 1:1000 and 1:1000, respectively. After overnight incubation the membranes were washed three times for 10 minutes in TBS-T and then incubated with mouse secondary antibodies (Cat # 715-035-150, Jackson ImmunoResearch) for one hour at room temperature. The membranes were washed three times for 10 minutes in TBS for 5 minutes. For detection of the proteins, the membranes were incubated with 10 ml of Amersham ECL Western Blotting Detection Reagent (Cat # RPN2106, GE) prepared according to manufacturer's instructions for 1 minute. In a dark room, the nitrocellulose membrane and film (Cat # 28906837, GE) were placed in a cassette. For reference, the exposure for UCP1 was 1.5 hours. The film was developed in a table-top developing machine (Curix 60, Afga Healthcare).

Insulin measurement

Blood collected from the tail vein was used to measure fasting insulin when the mice were 16-weeks old. Insulin levels were measured on a BioPlex analyser (Bio-Rad) using the Mouse Metabolic Magnetic bead panel kit (Cat # MMHMAG-44K, Millipore). The IPGTT and insulin measurement were performed after an overnight fast (16-hours) during the light period.

Culture of Sult1a1 primary adipocytes, transcriptomics and data analysis

Primary cultures of adipocytes were prepared from the iWAT of 19-week old WT and 33-week old Sult1a1 KO male mice. The SVF was collected as previously described (44) and then frozen in 80% DMEM (Sigma), 20% FBS and 10% DMSO until platting. The preadipocytes were seeded at a density of 2.5 x 10^4 cells/cm^2 in 6-well plates in plating medium which contained DMEM/F12 (Cat # 11320033, Gibco), 1% Penicillin-Streptomycin (10,000 U/mL) (Cat # 15140122, Gibco) and 10 % FBS (Cat # 11573397, Gibco). After the cells were 100 % confluent they were cultured as previously described (45) with the following modifications to the protocol: the differentiation medium contained 0.5 µM dexamethasone (Cat # D1756, Sigma Aldrich), 0.5 mM isobutylmethylxanthine (Cat # I5879, Sigma Aldrich), 170 nM insulin (Cat # I1507, Sigma Aldrich), and 1 µM rosiglitazone (Cat # 71740, Cayman). After 48 hours, the differentiation medium was replaced with induction medium which contained plating medium with 170 nM insulin and 1 µM rosiglitazone. The medium was refreshed every two days and the cells were harvested 10 days after addition of differentiation medium, washed twice with PBS and snap frozen until RNA extraction. The cells were lysed in 600 µl of lysis buffer with proteinase K and heated at 37 ˚C for 25 minutes in a heating block and then stored at -20 ºC until RNA extraction. RNA was extracted using Agencourt RNAdvance Tissue Kit (Beckman Coulter) according to the manufacturer's protocol. The QuantSeq 3′ mRNA sequencing technique (46) was performed by the Genomics Factory at the Nestlé Institute of Health Sciences using the QuantSeq 3' mRNA-Seq Library Prep Kit (FWD) HT for Illumina (Lexogen) and 50 ng of RNA. The sequencing data was filtered to exclude genes with low expression (< 20 counts). Differential expression analysis was performed by the Genomics Factory with edgeR (a Bioconductor package for R) to compare the expression of male WT and Sult1a1 KO mice. Pathway analysis on the differentially expressed genes was performed with Ingenuity Pathway Analysis (IPA) software.

Adipose tissue histology

The right eWAT depot was collected and weighted and then fixed in formalin (Leica), paraffin embedded and dehydrated in a gradient of 70, 95 and 100% ethanol. The tissue was incubated in Sub-X (Leica) before embedding in paraplast (Leica). The eWAT blocks were sectioned 7 µm thick with three sections per slide. Slides were stained with hematoxylin and eosin (H&E) and Sirius red (SR) according to standardized protocols of the EPFL Histology Platform. Images were acquired using a slide scanner (VS-120, Olympus) and scale bars were added using Fiji (ImageJ) software.

Sult1a1 substrate tissue accretion

Tissue accretion studies were performed on WT and Sult1a1 KO mice and received ethical authorization from the animal studies committee at the Nestlé Institute of Health Science and the French Ministry of Research under authorization number 2018092113188108 and 201711241419725. Experiments were performed in compliance with the European Community regulation for laboratory animal care and use (Directive 2010/63/UE).

Mice had *ad libitum* access to food (Safe, D04) and water and maintained on a 12 hour light/dark cycle at a temperature between 20-24°C and a relative humidity between 50-60%. WT mice in the time course experiment were male FVB/NHanHsd mice aged six weeks old and were obtained from Envigo (Horst aan de Maas, the Netherlands). After one week acclimatization, the mice were divided into four groups which represented a sampling time: group 1 (before resveratrol dosing), group 2 (10 minutes after dosing), group 3 (30 minutes after dosing) and group 4 (60 minutes after dosing) with six mice per group. Mice aged seven weeks old were fasted overnight and then received 240 mg/kg body weight resveratrol or vehicle by gavage at a rate of 10 ml/kg body weight. Resveratrol powder (Cat # RSXOL9800, Veri-te resveratrol, Evolva) was solubilized in PEG E 400 (Cat # 06855, Sigma Aldrich) to 90 mg/ml and mixed overnight. The solution was diluted to 24 mg/ml with water containing 15% DMSO (Cat # D2650, Sigma Aldrich) and mixed for one hour previous to administration.

After dosing, the mice were anesthetized with isoflurane and then blood was collected in heparin coated tubes from the retro-orbital site. After blood sampling, the mice were killed by cervical dislocation and tissues were collected. Blood and plasma were snap frozen in liquid nitrogen and stored at -80ºC until analysis.

In a second experiment, 11 male WT and Sult1a1 KO mice were dosed with resveratrol or vehicle (DMSO only) which was prepared as previously described. 20 minutes after resveratrol dosing, the mice were anesthetized and blood was collected. The mice were killed by cervical dislocation and then the following tissues were collected: eWAT, liver, kidney, skeletal muscle (gastrocnemius). Tissues and plasma were snap frozen in liquid nitrogen and stored at -80ºC until analysis.

UHPLC-UV analysis of resveratrol and metabolites in WT and Sult1a1 KO mice

Standards, chemicals, preparation of standards, preparation of mobile phase and UHPLC-UV settings used for analysis are described in **Extended Materials and Methods**. The method used to measure resveratrol and its metabolites was developed through a collaboration with Prof. Karen Brown and Dr. Hong Cai at the University of Leicester.

Sample preparation

eWAT was homogenized with three parts of 50 mM HEPES buffer. Each homogenate (150 µL) was spiked with 1.5µL of 0.2mg/mL internal standard (3-hydroxy-4'-methoxystilbene) and was then mixed with 450 µL acetonitrile. The mixture was loaded onto a 3 mL preconditioned lipid clear-up cartridge and eluted with 300 µL of 20% HEPES in acetonitrile, followed by 225 µL of 100% acetonitrile. The eluent solvent was evaporated under nitrogen then reconstituted with 150 µL of MeOH and H2O (1:1, v/v). A 20µL volume of the supernatant was injected onto the HPLC column for analysis.

Liver samples were prepared by homogenizing one part liver tissue (50 mg) with 19 parts of 50 mM HEPES buffer and acetone (2:3, v/v) (950 µl). Naringenin internal standard (2 µL of 1.25 mg/mL) was spiked into 200 µL of liver homogenate. The samples were vortex mixed for 1 minute and then chilled at -20ºC for 10 minutes. The samples were centrifuged at 13,000g, 4 °C for 10 min. 150 µL of the supernatant was removed and dried under nitrogen. The residue was reconstituted with 100µL of MeOH and H2O (1:1,v/v) and 10 µL was injected onto the column.

Plasma samples were prepared as described in **Extended Materials and Methods** with the following modification to the protocol: 10 µL, rather than 30 µl, of sample was injected onto the HPLC column, samples were measured in duplicates.

For the preparation of kidney, muscle and colon 7.5 parts of 50 mM HEPES /acetone (2:3) was added to one part tissue and then homogenized. The homogenate (375µL) was spiked with 15 µL of 0.1 mg/mL

internal standard (naringenin) and centrifuged at 13,000g (4°C) for 10 minutes then 250 µL of the supernatant was removed and concentrated to dryness under nitrogen. The residue was reconstituted in 100µL of MeOH and H2O (1:1, v/v). A 20µL volume of the resulting solution was injected onto the HPLC column.

Data Analysis

The peak area ratio for each metabolite was calculated for each metabolite and was divided by the peak area ratio of the internal standard to correct for losses during sample manipulation.

3. Results

3.1. Characterization of the Sult1a1 KO mouse on a standard diet

Growth and development of the Sult1a1 KO strain has not been described in the literature and caretakers at the DIfE and Phenomin-Mouse Clinic Institute both confirm no obvious macroscopic differences between WT and Sult1a1 KO mice. Knockout of Sult1a1 is not lethal and litter size is similar between the WT and KO strain with an average 6.9 and 6.0 pups born per litter, respectively (**Supplementary Table 2**). Previously the liver transcriptome of WT and Sult1a1 KO mice was compared with no major differences observed in gene expression with the exception of Sult1a1 in the KO strain (communication with Glatt Lab at the DIfE). Adipose tissue from the Sult1a1 KO mice has not been previously characterized.

To determine if SULT1A1 contributes to the constitutionally thin phenotype, Sult1a1 KO mice were characterized. The body weight of male WT controls and Sult1a1 KO mice was tracked weekly from the age of 6 to 20 weeks old. At 6 weeks old, a 2.3 g difference in body weight was already apparent between WT (24.94 ± 0.4473 g) and Sult1a1 KO (22.59 ± 0.3261 g) which was statistically significant. Throughout the study, Sult1a1 KO mice weighed persistently less than WT mice. At 20 weeks old, WT mice (37.15 ± 1.31 g) weighed significantly more than Sult1a1 KO mice (31.14 ± 0.8022 g) (**Fig. 2A**).

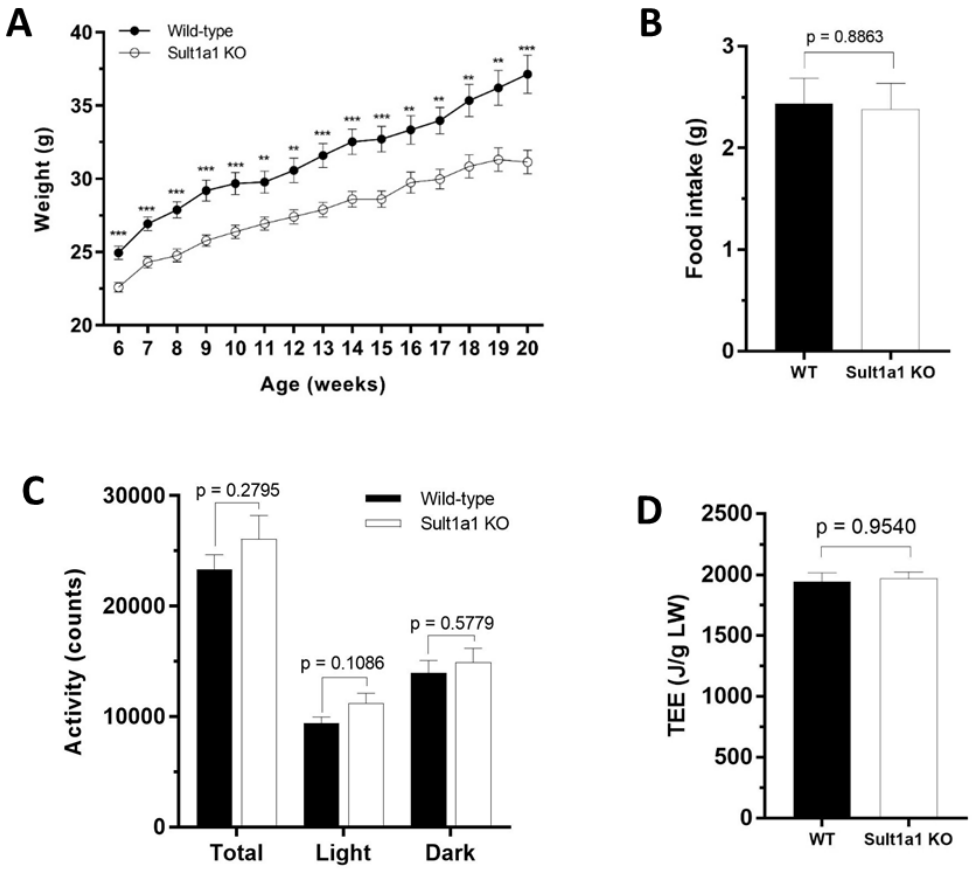

Fig.2: Sult1a1 KO mice have reduced body weight.

A. Body weight of wild-type and Sult1a1 knockout mice on a standard diet for 14-weeks (n = 11-15 at each time point). Data represented as mean ± SEM. p values were calculated using an unpaired Student's t test at each time point **p ≤ 0.01 and *** p ≤ 0.001.

B. 24-hour food intake of mice housed in metabolic cages at 14-weeks old (n = 14-15 per genotype). p value was calculated using an unpaired Student's t test. Data represented as mean ± SEM.

C. 24-hour activity of mice housed in metabolic cages at 14-weeks old (n = 14 per genotype). Total activity was divided into activity during the light and dark phase to check for differences between the genotypes. p values were calculated using an unpaired Student's t test. Data represented as mean ± SEM.

D. TEE of mice housed in metabolic cages at 14-weeks old (n = 13-15 mice per time point). TEE in units J/h/g LW (lean weight). p value was calculated using an unpaired Student's t test. Data represented as the mean ± SEM.

When the mice were 14 weeks old, VO_2, VCO_2, food intake and activity were recorded for 48-hours using the TSE PhenoMaster System. Data analysis was performed on the last 24-hours of recording. Food intake over 24-hours was not significantly different between the groups (WT = 2.44 ± 0.93 g vs Sult1a1 KO = 2.39 ± 0.90 g) (**Fig. 2B**) nor was total 24-hour activity (WT = 23441.01 ± 4975.53 counts vs Sult1a1 KO = 26094.79 ± 2109 counts) (**Fig. 2C**) indicating that changes in food intake and activity do not account for the reduced body weight of Sult1a1 KO mice.

VO_2 and VCO_2 values were allometrically scaled to lean body mass using the TSE software. From the hourly VO_2 and VCO_2 values, EE per hour was calculated and summed to determine the total energy expenditure (TEE) shown in **Fig. 2D**. TEE was not significantly different between WT (1943 ± 72.99 J/g lean weight) and Sult1a1 KO mice (1968 ± 54.92 J/g lean weight). Unadjusted EE values are shown in **Supplementary Fig. 2**. Body composition was measured using qNMR and conducted directly after EE measurement (**Supplementary Fig. 3**). Sult1a1 KO mice had 14% reduction in lean mass and 18% reduction fat mass which was statistically significant (**Supplementary Fig. 3A**). To adjust EE for differences in lean body weight, analysis of covariance (ANCOVA) was performed. Linear regression of unadjusted EE values and lean body weight indicated that the genotypes have different associations between lean body weight and EE (i.e. slopes of the regression lines were different) (**Supplementary Fig. 4A**) preventing the use of ANCOVA and indicating that EE should be adjusted using alternative methods. Regression of EE and total body weight yielded similar results (**Supplementary Fig. 4B**).

At 16-weeks old, the glycaemia of WT and Sult1a1 was evaluated using an intraperitoneal glucose tolerance test (IPGTT). Insulin secretion was measured during the IPGTT. At 18-weeks old, an intraperitoneal insulin tolerance test (IPITT) was performed. Glucose tolerance, insulin secretion and insulin sensitivity were similar between WT and Sult1a1 KO mice (**Supplementary Fig. 5**)

3.2. Molecular characterization of adipose tissue from Sult1a1 KO mice on a standard diet

Since metabolic phenotyping of the Sult1a1 KO line offered no obvious explanation for the reduced body weight phenotype, the adipose tissue was further characterized as SULT1A1 was reduced in CT adipose tissue. Specifically, the respiratory capacity of adipocytes was measured as a previous study identified an increase in the mitochondrial respiratory capacity of CT adipocytes (7). The respiratory capacity of WT and Sult1a1 KO adipocytes was measured using high-resolution respirometry. Representative subcutaneous

(iWAT) and visceral (eWAT) depots were selected for measurement and from these depots adipocytes were isolated and respiratory capacity was recorded using the Oroboros.

Intact primary adipocytes isolated from the iWAT had increased basal, leak and maximal respiration (**Fig. 3A**) with a statistically significant increase ($p = 0.0019$) in leak respiration in Sult1a1 KO adipocytes (WT = 46.02 ± 5.32 pmol/s · mg DNA vs Sult1a1 KO = 146.3 ± 18.69 pmol/s · mg DNA) The cellular respiratory control ratio (cRCR), a measure of mitochondrial integrity, was not significantly different between the genotypes (**Fig. 3B**) indicating that mitochondrial integrity is similar between the groups. Since Sult1a1 KO mice had an increase in leak respiration and leak respiration can be driven by Ucp1, its expression was measured from the same adipocytes shown in **Fig. 3A**. Ucp1 expression was increased in the iWAT of Sult1a1 KO mice (**Fig. 3C**) confirming the brown appearance of the iWAT collected from Sult1a1 KO mice (**Supplementary Fig. 6**). Voltage-dependent anion-selective channel 1 (VDAC), a protein of the outer mitochondrial membrane was measured and was increased in the iWAT tissue of Sult1a1 KO mice (**Fig. 3D**) indicative of increased mitochondrial content in the iWAT depot of Sult1a1 KO mice.

Intact primary adipocytes from the eWAT depot had a higher but not statistically significant increase in basal and maximal respiratory capacity (**Supplementary Fig. 7**). Leak respiration in adipocytes isolated from eWAT was similar between the genotypes suggesting that the browning phenotype is specific to the iWAT depot of Sult1a1 KO mice. In summary, Sult1a1 KO mice have a reduced body weight in comparison to WT mice. The subcutaneous adipose tissue of Sult1a1 KO mice has increased leak respiration, increased Ucp1 expression and increased mitochondrial content indicating browning of Sult1a1 KO subcutaneous adipose tissue.

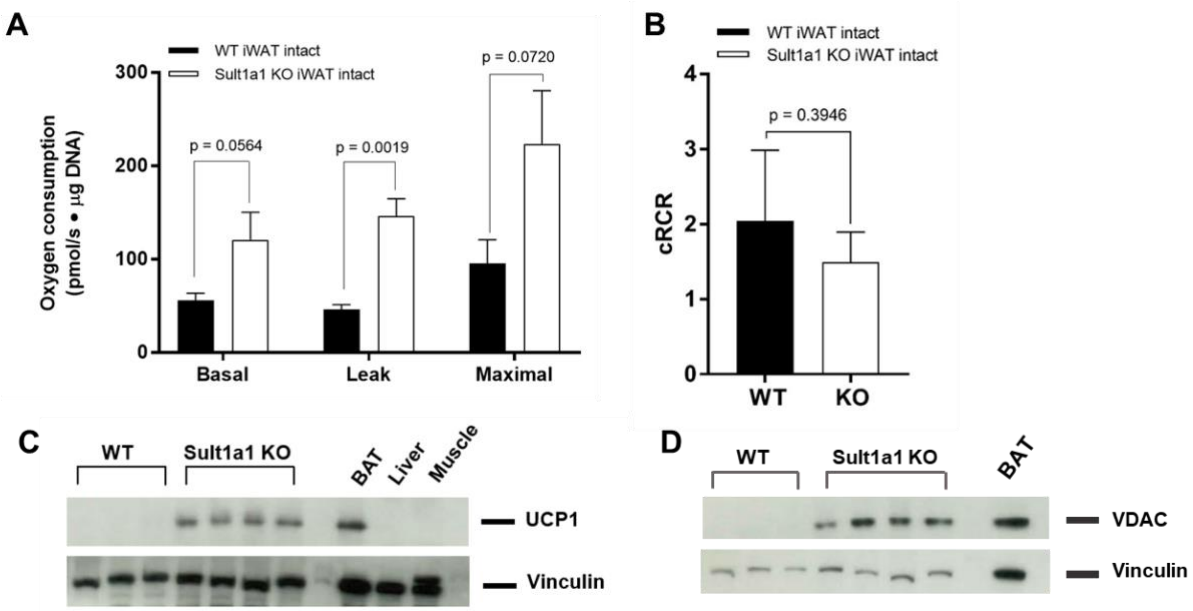

Fig. 3. Loss of Sult1a1 increases leak respiration and expression of mitochondrial proteins in iWAT

A. Higher respiratory capacity in intact subcutaneous adipocytes (iWAT) from Sult1a1 knockout mice (n = 3-4). Basal respiration was measured using pyruvate (5µM) and malate (5µM) as a substrates. Leak respiration was measured by inhibiting ATP synthase with oligomycin (2µg/ml). Titration of FCCP (0.5 µM steps) was used to determine maximal respiration. Non-mitochondrial respiration was measured by adding antimycin A (2.5 µM) and subtracted from all other respiratory states. Oxygen consumption was normalized by µg of DNA per chamber. Data represented as mean ± SEM. p values were calculated by using an unpaired Student's t test.

B. No difference in mitochondrial integrity of intact iWAT from Sult1a1 KO and WT mice. The cRCR was calculated by dividing maximal respiration by leak respiration. Data represented as mean ± SD. p value was calculated by using an unpaired Student's t test.

C. Western blot using anti-UCP1 antibody on protein lysates isolated from iWAT analyzed in Fig. 3A. Vinculin serves as loading control. First three lanes are wild-type iWAT lysate followed by four Sult1a1 knockout iWAT lysate. The last three lanes are controls; BAT serves as positive control and expresses UCP1 protein, liver and muscle serve as negative control and do not express UCP1.

D. Western blot using anti-VDAC antibody on protein lysates isolated from iWAT analyzed in Fig. 3A. Vinculin serves as loading control. First three lanes are wild-type iWAT lysate followed by four Sult1a1 knockout iWAT lysate. The last lane is BAT which serves as positive control for mitochondrial protein expression.

3.3. Characterization of Sult1a1 KO mice on a high-fat diet (HFD)

Since CT individuals are resistant to weight gain even when food intake is increased beyond their energy requirement (10), it was hypothesized that Sult1a1 KO mice would be resistant to weight gain as well. To test this hypothesis, Sult1a1 KO mice were provided with a HFD for 13-weeks. This experiment was conducted on weight matched WT and Sult1a1 KO mice. At 7-weeks old, the mice were switched from house chow (8.4% kcal from fat) to a HFD (45% kcal from fat). After 13-weeks on a HFD Sult1a1 KO mice had a significantly lower body weight than controls (WT = 45.48 ± 0.5981 g vs Sult1a1 KO = 42.98 ± 0.7655 g, p = 0.02) (**Fig. 4A**) recapitulating the weight resistance phenotype of CT individuals.

We investigated if this resistance to weight gain could provide protection against the harmful effects of diet induced obesity. At 16-weeks old, after 9 weeks on a HFD, Sult1a1 KO mice had significantly lower concentrations of insulin after fasting in comparison to WT controls (**Fig. 4B**) (WT = 1.797 ± 0.2947 µg/l; Sult1a1 KO = 1.011 ± 0.2321 µg/l). Fasting blood glucose was lower in Sult1a1 KO mice but did not reach statistical significance (**Supplementary Fig. 8A**). The blood glucose time course was similar after intraperitoneal (IP) injection of glucose (**Supplementary Fig. 8B**) and the AUC from 0 to 120 minutes was lower in KO mice but not statistically different between the genotypes (**Supplementary Fig. 8C**). Blood insulin levels during the glucose tolerance test were not statistically different 15 and 30 minutes after IP injection of glucose (**Supplementary Fig. 8D**) indicating that glucose stimulated insulin secretion is similar between the genotypes and that the differences observed in the glucose tolerance test are driven by preserved insulin sensitivity rather than differences in insulin output. The insulin tolerance test was performed to evaluate insulin sensitivity. At 18-weeks old, after 11 weeks on a HFD, Sult1a1 KO mice tended to have lower blood glucose in response to IP injection of insulin throughout the test (**Supplementary Fig. 8E**) and AUC from 0 to 120 minutes was lower in Sult1a1 KO mice but not statistically significant (**Supplementary Fig. 8F**).

To understand the contribution of adipose tissue to insulin sensitivity, adipose tissue from WT and Sult1a1 KO mice was examined. Total body fat measured by qNMR was similar between the genotypes and visceral fat pad weight (eWAT and rWAT) tended to be higher in the in the Sult1a1 KO but was not statistically significant (**Fig. 4C**). Since excess visceral adipose tissue is correlated with increased risk of insulin resistance (47), the adipose tissue of WT and Sult1a1 KO mice was further examined. Transcriptomics on

primary adipocytes isolated from the iWAT of both genotypes and differentiated in vitro indicated that Sult1a1 KO mice have an anti-inflammatory phenotype (**Table 3**). Pathway analysis on the differentially expressed genes indicated a significant enrichment of genes annotating to the complement system and acute phase signaling. Genes coding for proteins of the complement cascade (C1R, C2 and C3) were significantly downregulated in the primary cells of Sult1a1 KO mice. Additionally, the dataset also showed a downregulation of LBP which binds LPD, a proinflammatory molecule (48).

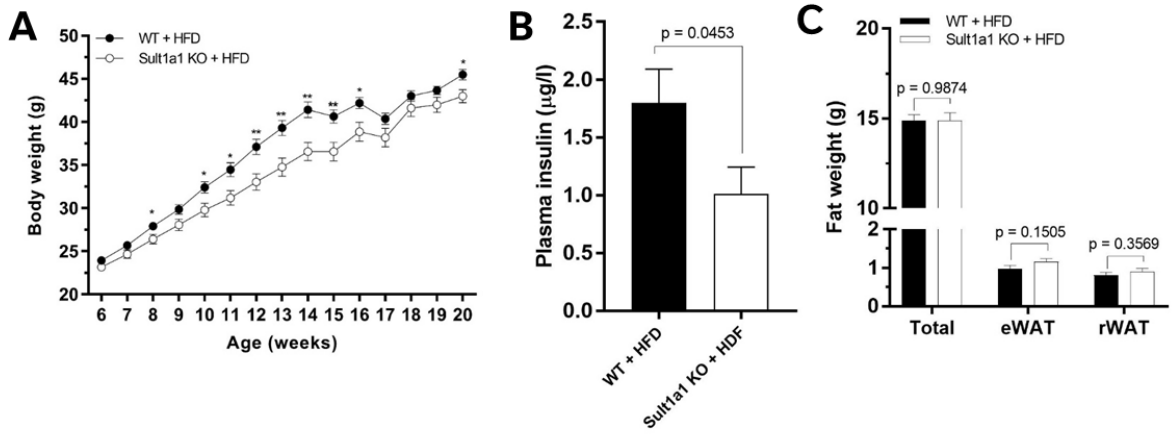

Fig. 4. Sult1a1 KO mice are resistant to weight gain and have preserved insulin sensitivity

- **A.** Body weight of WT and Sult1a1 KO mice on a HFD for 13-weeks. (n = 14-15 for WT and n = 15 for Sult1a1 KO at each time point). Data represented as mean ± SEM. p values were calculated using an unpaired Student's t test *p ≤ 0.05 and **p ≤ 0.01
- **B.** Fasting plasma insulin levels of WT and Sult1a1 KO mice 14-weeks old (WT = 1.797 ± 0.2947 µg/l, Sult1a1 KO = 1.011 ± 0.2321 µg/l; p = 0.0453, n = 15 for both genotypes). p value was calculated using an unpaired Student's t test. Data represented as mean ± SEM
- **C.** Fat weight of WT and Sult1a1 KO mice on a HFD for 13-weeks. Total body fat was measured by qNMR). eWAT and rWAT fat pads were dissected and weighed. n = 14 for WT mice and n = 15 for Sult1a1 KO. p value was calculated using an unpaired Student's t test. Data represented as mean ± SEM

Table 3: Enriched pathways in primary adipocytes from Sult1a1 KO mice

Ingenuity Canonical Pathways	p-value	Overlap	Transcripts
LXR/RXR Activation	1.55E-05	4.1%, (5/121)	APOE,C3,CLU,KNG1,LBP
Complement System	1.20E-04	8.1%, (3/37)	C1R,C2,C3
FXR/RXR Activation	3.24E-04	3.2%, (4/126)	APOE,C3,CLU,KNG1
Atherosclerosis Signaling	3.31E-04	3.1%, (4/127)	APOE,CLU,COL1A1,TNFRSF12A
Acute Phase Response Signaling	1.20E-03	2.2%, (4/175)	C1R,C2,C3,LBP

Histology on eWAT sections from mice on a HFD confirmed the anti-inflammatory phenotype of Sult1a1 KO primary adipocytes. H&E stained sections of eWAT were strikingly different between the genotypes. eWAT sections from WT mice had darkly stained patches which surrounded large circles while eWAT from Sult1a1 KO mice had fewer dark patches and classical white adipocyte morphology (**Fig. 5**). Inspection of the eWAT sections confirmed that the darkly stained patches were infiltrated with immune cells and that the large symmetrical circles were lysed adipocyte remnants. eWAT sections were also stained with Sirius red (SR) which binds to collagen (49). In comparison to Sult1a1 eWAT, sections from WT mice on a HFD had increased collagen deposition indicative of adipose tissue fibrosis suggesting that Sult1a1 KO mice are protected from adipose tissue fibrosis (**Fig. 6**). In summary, under HFD conditions eWAT from Sult1a1 KO mice is protected from immune cell infiltration, inflammation and fibrosis while WT adipose tissue has a proinflammatory phenotype, a hallmark of insulin resistance.

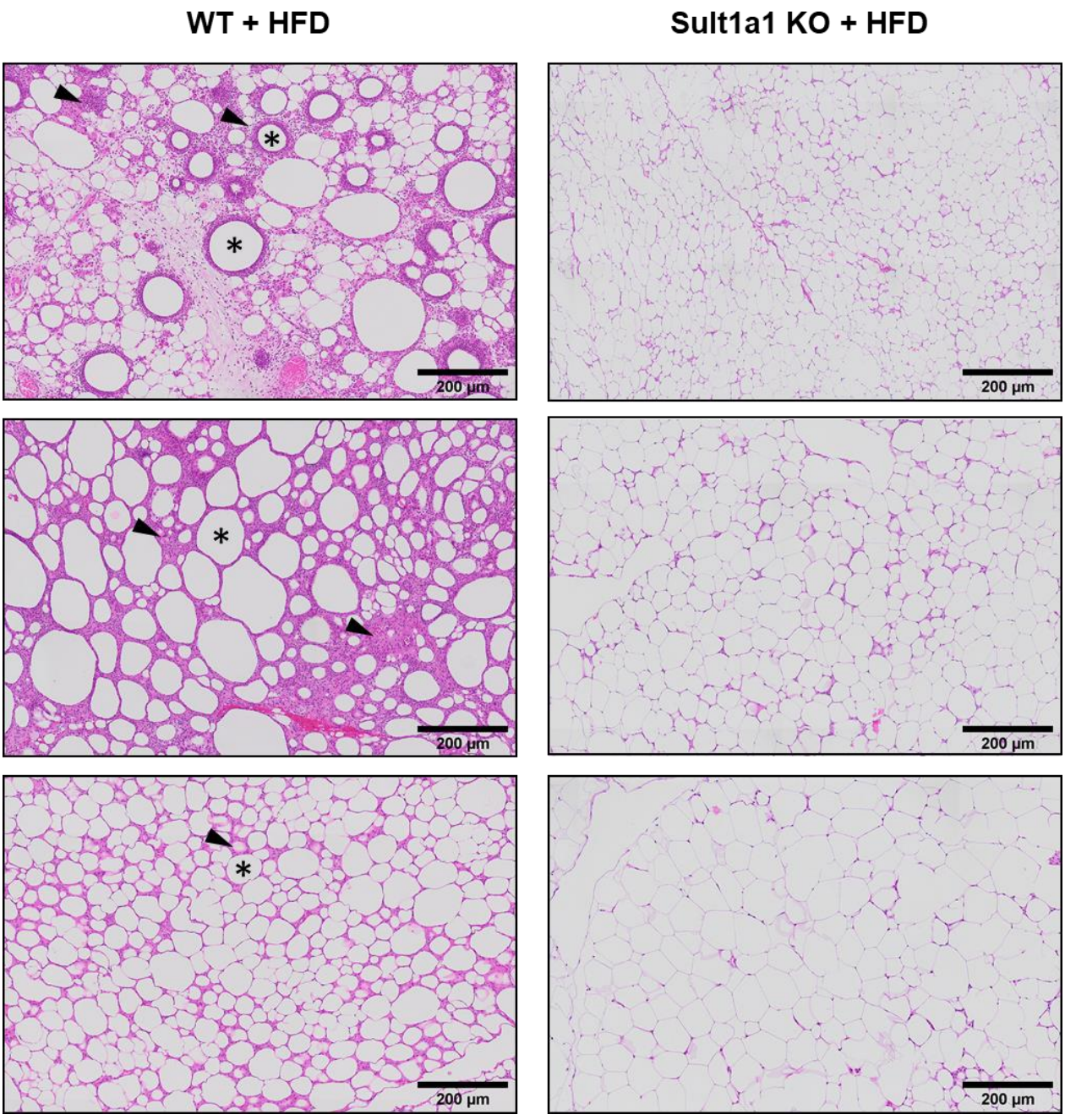

Fig. 5: Sult1a1 KO mice are protected from immune cell infiltration and inflammation on a HFD. Representative images of H&E stained eWAT from WT and Sult1a1 KO mice on a HFD for 13 weeks. Each image was taken from a different mouse, n = 3 per genotype. Arrowheads indicate immune cell infiltration and stars indicate lysed adipocyte remnants.

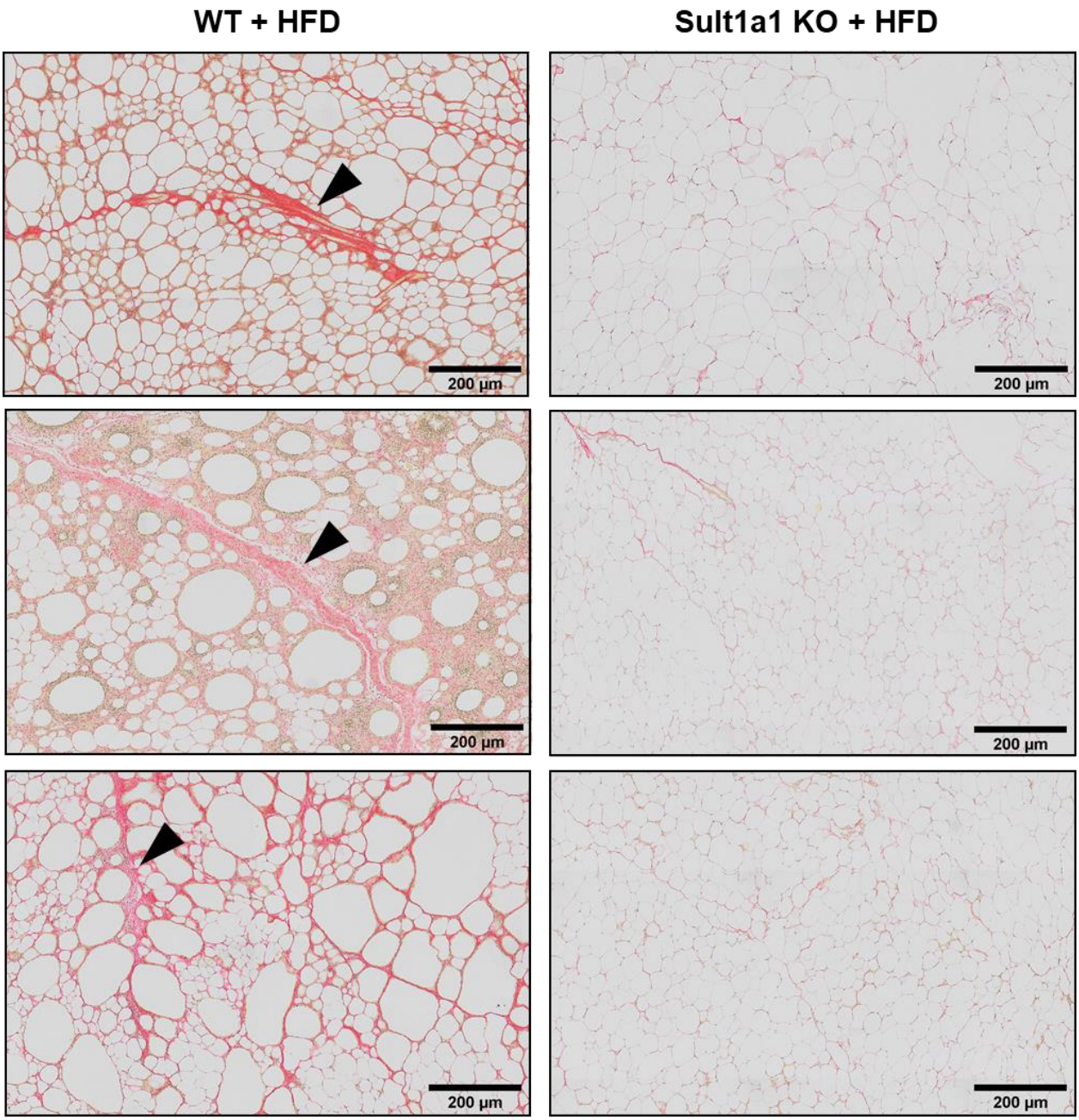

Fig. 6: Reduced adipose tissue fibrosis in Sult1a1 KO mice on a HFD. Representative images of SR stained eWAT from WT and Sult1a1 KO mice on a HFD for 13 weeks. Each image was taken from a different mouse, n = 3 per genotype. Arrowheads indicate collagen deposits.

Non-alcoholic fatty liver disease (NAFLD) is associated with insulin resistance and is characterized by ectopic accumulation of triglycerides in liver tissue. TG accumulation in the liver is a consequence of insulin resistance which impairs the ability of adipocytes to store lipids. As a result, the liver is exposed to increased

TG which accumulate within the liver and trigger triglyceride synthesis and *de novo* lipogenesis (DNL) further exacerbating insulin sensitivity (50). Sult1a1 KO mice had a significantly reduced liver weight (**Supplementary Fig. 9A**). Adjustment of liver weight to account for size differences by ANCOVA was not possible as the linear relationship between liver weight and total body weight was different between the genotypes (**Supplementary Fig. 9B**). A similar linear relationship was observed between liver weight and lean body weight (**Supplementary Fig. 9C**)**.**

A factor that could account for reduced liver weight is reduced TG accumulation in the livers of Sult1a1 KO mice. To quantify TG accumulation, liver sections were stained with Oil Red O which binds to neutral lipids, like TGs, and stains them red. The results of the Oil Red O stain quantification were inconclusive as the stain only partially coated the lipid droplet making it difficult accurately identify lipid droplets and quantify the stain (**Supplementary Fig. 10**). H&E stained sections did not show any obvious differences between the genotypes on a HFD (**Supplementary Fig. 11**). The hypothesis that Sult1a1 liver weight is reduced due to reduced triglyceride accumulation aligns well with the tendency for Sult1a1 KO mice to have preserved insulin sensitivity. However, experiments to accurately quantify liver triglyceride content are needed to confirm this hypothesis.

3.4. Molecular mechanisms underlying the Sult1a1 KO mouse phenotype

Phenotyping of the Sult1a1 KO mouse line indicates that loss of Sult1a1 reduces body weight and that absence of Sult1a1 triggers adipose tissue browning. On a HFD for 13 weeks Sult1a1 KO mice are resistant to weight gain and less susceptible to diet induced obesity indicated by preserved insulin sensitivity and reduced adipose tissue inflammation. However, the molecular mechanism underlying these observations remains unclear. To gain insight, transcriptomics on primary adipocytes from the iWAT depot of male mice were collected and differentiated in vitro. From mature primary adipocytes, RNA was collected for 3' RNA-sequencing. DEG analysis compared the expression of transcripts from male Sult1a1 KO mice and WT mice. DEG analysis identified 59 genes using a significance level of $p = 0.05$ on the adjusted p-value. Pathway analysis on the 59 genes showed a significant enrichment of genes annotating to LXR/RXR Activation, Complement System, FXR/RXR Activation, Atherosclerosis Signaling and Acute Phase Response Signaling (**Table 3**). The most significantly enriched pathway was liver X receptor (LXR)/RXR

activation ($p = 1.55 \times 10^{-5}$). Based on the directionality of the transcript fold-change, IPA software predicted downregulation of the LXR/RXR pathway.

The LXR/RXR pathway was also identified in a separate dataset using the Simpson-Golabi-Behmel syndrome (SGBS) cell line, a model for human adipocytes (51). In this experiment, SGBS cells were transfected with either scramble siRNA (control) or siRNA targeting SULT1A1 (SULT1A1 knockdown) and then gene expression was compared between control and SULT1A1 knockdown adipocytes. In the SGBS dataset, IPA software also predicted downregulation of the LXR/RXR pathway. To the LXR/RXR pathway NR1H3, the gene coding for the LXRα nuclear receptor, was downregulated in SGBS cell line (**Supplementary Figure 12**).

Since the LXR/RXR pathway was identified in both the mouse primary adipocytes and a human adipocyte cell line, it was hypothesized that loss of Sult1a1 modulates the sulfonation of substrates which downregulate the LXR/RXR pathway. The main substrate for LXR are oxysterols, oxidized derivatives of cholesterol, which are typically sulfonated by the SULT2 family of enzymes (52). As the sulfotransferase family of enzymes share similarities in the PAPS binding domain and catalytic sites, the affinity of oxysterols for SULT1A1 was measured using a radiochemical assay to determine if oxysterols are substrates for SULT1A1.

Four oxysterols, 25-hydroxycholesterol, 7-ketocholesterol, 24(S)-hydroxycholesterol and 22(R)-hydroxycholesterol, were tested using a radiochemical assay which used S-35 labelled PAPS. In the presence of the SULT1A1 enzyme and a SULT1A1 substrate, the radiolabeled S-35 from PAPS will integrate into the SULT1A1 substrate. Radiolabeled substrates will emit beta particles that are detected by a counter which records the number of beta particle counts per minute (cpm). As a positive control known SULT1A1 substrates like p-NP and resveratrol were used to compare the affinity of oxysterols towards SULT1A1 which have cpm values that range from 14000 - 20000. In the presence of the SULT1A1 enzyme S-35 PAPS and 25-hydroxycholesterol the cpm values ranged from 3134.5 to 2499.5 for the concentrations tested. The 25-hydroxycholesterol cpm was not significantly different from the vehicle (cmp = 2530.5) which indicates that 25-hydroxycholesterol is not a substrate for SULT1A1 (**Supplementary Fig. 13A**). Similar

results were observed for the 7-ketocholesterol, 24(S)-hydroxycholesterol and 22(R)-hydroxycholesterol (**Supplementary Fig. 13B-D)**

In summary, downregulation of the LXR/RXR pathway was represented in two independent datasets from primary mouse adipocytes and a human cell line. Since the LXR/RXR pathway is stimulated by oxysterols, the affinity of oxysterol affinity to SULT1A1 was tested using a radiochemical assay. The results of the radiochemical assay indicate that SULT1A1 does not sulfonate the oxysterols tested.

3.5. Metabolism of Sult1a1 substrates in Sult1a1 KO mice

In the previous experiment the affinity of unknown substrates (oxysterols) towards SULT1A1 was tested. The following experiments tested how loss of Sult1a1 affects the metabolism of known substrates. The known substrate used in the following experiments was resveratrol. Since Sult1a1 metabolism in the adipose tissue was the most relevant for understanding the CT phenotype, a time course experiment was performed to determine if resveratrol, a Sult1a1 substrate, can be detected in the adipose tissue.

Table 4 shows the concentration of resveratrol and its major metabolites measured in the adipose tissue of WT mice dosed with 240 mg/kg body weight resveratrol at 10, 30 and 60 minutes. In WT adipose tissue, resveratrol and its metabolites can be detected and measured which has not been previously demonstrated in mice.

Table 4: Concentration of resveratrol and its main metabolites in mouse adipose tissue 10, 30 and 60 minutes post dosing with 240 mg/kg body weight resveratrol

Analyte (ng/g ± SEM)	10 minutes	30 minutes	60 minutes
Resveratrol	3594.1 ± 1165.5	158.0 ± 110.1	24.3 ± 15.5#
Resveratrol-3-sulfate	971.5 ± 191.8	1388.5 ± 259.8	846.6 ± 244.7
Resveratrol-4'sulfate	48.5 ± 23.0	106.3 ± 28.4	39.9 ± 14.7
Resveratrol-3 glucuronide	10031.3 ± 772.7	9583.5 ± 2524.4	5063.5 ± 1436.2
Resveratrol-4'-glucuronide	113.2 ±7.4#	93.5 ± 31.0#	ND

# indicates concentrations that are below the LDL, ND = not detected

After confirming the accretion of resveratrol in the adipose tissue, in a second experiment WT and Sult1a1 KO mice were dosed with 240 mg/kg body weight resveratrol and tissues were collected 20 minutes post-dosing based on the time course previously performed on WT mice. Loss of Sult1a1 tended to increase

resveratrol accretion in the tissues of Sult1a1 KO mice. In the plasma, there was a 2.2 fold increase in resveratrol concentration (**Fig.7A**). The adipose (eWAT), muscle (gastrocnemius), liver and colon had 1.7 fold increase in resveratrol (**Fig. 7B-E**, respectively). The largest increase in resveratrol accretion was observed in the kidney which had an approximately 5 fold increase in resveratrol concentration which was statistically significant (p = 0.0006) (**Fig. 7F**).

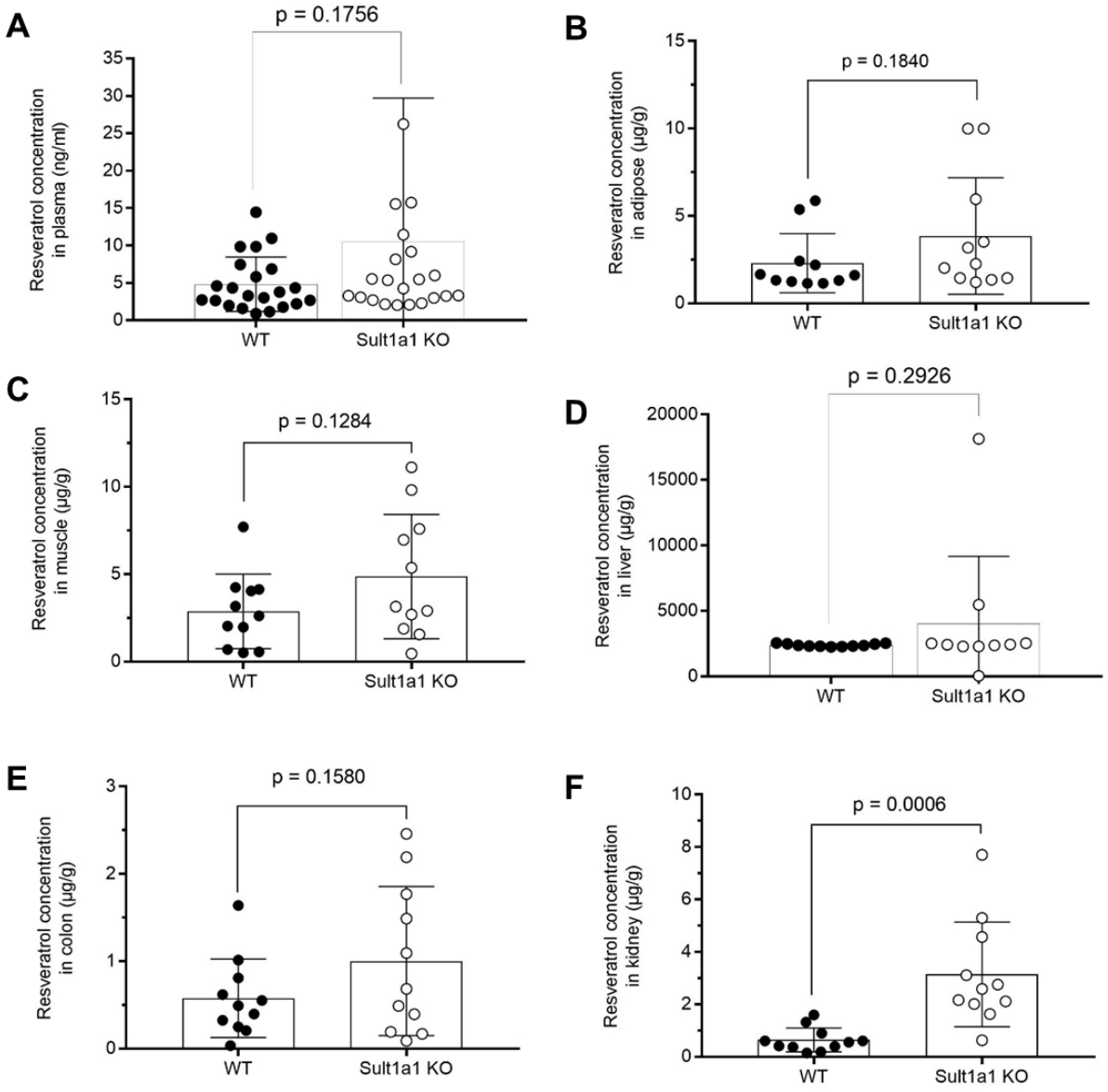

Fig. 7: Loss of Sult1a1 increases substrate acceretion in tissues. Resveratrol concentration in (**A**) plasma (**B**) adipose (eWAT) (**C**) muscle (**D**) liver (**E**) colon and (**F**) kidney and of WT (black dots) and Sult1a1 knockout mice (white dots). Mice were dosed with 240 mg/kg body weight resveratrol. Tissues

were collected 20 minutes post-dosing. n = 9-11 mice per group, plasma measured in duplicates. Data presented as mean ± SD; p values were calculated by using an unpaired Student's t test.

Surprisingly, sulfonated metabolites were also detected in the tissues of Sult1a1 KO mice (**Supplementary Fig. 14**) indicating that there is some compensation by other sulfotransferases for the loss of Sult1a1. The liver was further investigated since in comparison to other tissues, liver highly expresses Sult1a1 (**Supplementary Fig. 15**) indicating an important role for Sult1a1 in liver function. Additionally, resveratrol-3-sulfate concentration was similar between WT and Sult1a1 KO mice suggesting compensation by other sulfotransferases. To identify compensatory sulfotransferases, mRNA expression of the entire sulfotransferase family was screened in the liver of WT mice. In the liver, the most abundantly expressed Sult family members are Sult1a1, Sult1b1 and Sult5a1 (**Supplementary Fig. 16**). In a follow-up experiment, mRNA expression of Sult1a1, Sult1b1 and Sult5a1 was measured in the liver tissue collected from the WT and Sult1a1 KO mice dosed with resveratrol. As expected, Sult1a1 was not detectable in the liver. However, a significant induction of Sult5a1 was observed in both WT and Sult1a1 KO mice implicating Sult5a1 in the production of resveratrol-sulfate metabolites in the liver. Vehicle treated mice had a significant increase in Sult1b1 suggesting that without substrate Sult1a1 KO mice may express more Sult1b1 basally (**Supplementary Fig. 17**).

Since adipose is the most relevant tissue for understanding the CT phenotype, mRNA expression of the sulfotransferase family was screened in the eWAT of WT mice. Sult1a1 is most abundantly expressed in the eWAT of WT mice followed by Sult1e1 and Sult5a1 (**Supplementary Fig. 16**). The results of the Sult mRNA screening indicate that pattern of Sult expression differs between tissues which may influence the sulfonation of substrates in a tissue specific manner. In summary, resveratrol was used as a model molecule to validate the use of the Sult1a1 KO model and demonstrate that loss of Sult1a1 results in decreased metabolism of a known substrate. Deletion of Sult1a1 tends to increase tissue accretion of resveratrol however resveratrol-sulfate metabolites were detectable in the tissues indicating compensation by other sulfotransferase family members.

4. Discussion

Constitutional thinness is a unique phenotype of human leanness and resistance to weight gain. Studies of lean and weight gain resistant individuals may complement our understanding of obesity by identifying factors that promote leanness and prevent weight gain. To gain insight into the mechanisms underlying the CT phenotype, the adipose tissue transcriptome of CT individuals and normal body weight controls were compared. SULT1A1 was the most downregulated transcript in the adipose tissue of the CT individuals. To understand the contribution of SULT1A1 towards the CT phenotype, a full body Sult1a1 KO mouse line was characterized on a standard diet and HFD.

Characterization of mice on a standard diet

On a standard diet, Sult1a1 KO mice weighed persistently less than WT mice throughout the study. During indirect calorimetry, feeding and movement of individually housed mice was tracked for 24-hours. Over the 24-hours, this study could not detect statistically significant differences in food intake or total physical suggesting that energy balance between the genotypes is similar and that differences in feeding and movement cannot account for the reduced body weight observed in Sult1a1 KO mice. To complement the food intake assessment, a future experiment could compare energy assimilation between the genotypes using bomb calorimetry to check for energy loss through feces.

A factor which could affect body weight are differences in litter size which can influence development as smaller litters have more access to food and maternal care while pups from larger litters tend to have less access to food and care (53). The mice in this experiment were derived from homozygous litters. Sult1a1 KO homozygous litters were on average smaller than WT homozygous litters suggesting that differences in litter size do not account for the reduced weight observed in Sult1a1 KO mice. A confounding factor that could influence development is the *in utero* environment which is a strong determinant of neonatal growth (53). To minimize the effect of *in utero* differences, future experiments should compare WT and Sult1a1 KO pups from heterozygous breeding pairs with similar litter size. The impact of Sult1a1 deletion on development should be addressed in future experiments by measuring body length and weight as soon as the pups can be handled.

EE was measured by recording the volume of O_2 consumed and CO_2 produced by the mice using the TSE LabMaster system. The TSE software can automatically adjust the volume of O_2 and CO_2 gas for differences in body weight or body composition using allometric scaling. In this study, the gas exchange data was scaled to lean body weight. This method of analysis showed no significant difference in EE between the genotypes.

The EE data was re-analyzed without the TSE allometric adjustment for lean body weight. This analysis showed that unadjusted EE is significantly lower in Sult1a1 KO mice. Since lean mass and EE are positively correlated (54), it was anticipated that Sult1a1 KO mice would have a lower EE as they have less lean mass. To control for differences in body weight or composition, several publications recommend adjusting the EE with a statistical method called ANCOVA (54–57). In preparation for ANCOVA, linear regression plots were analyzed to check that the data collected fit the assumptions of the statistical test. In this analysis, the slopes of the regression lines were different for each genotype, weakly correlated and intersected and thus did not meet the assumptions of the test. As the data did not fulfill the assumptions of ANCOVA, the analysis was inconclusive, an aspect that will be addressed again further on in the discussion.

In summary, Sult1a1 KO mice have a reduced body weight without changes in food intake or activity and without a clear change in energy expenditure. Since reduced SULT1A1 expression was observed in the adipose tissue of CT individuals and CT adipose tissue had increased mitochondrial activity (7), the respiratory capacity of adipocytes isolated from WT and Sult1a1 KO mice was measured using high resolution respirometry (Oroboros). Sult1a1 adipocytes isolated from iWAT had a significant increase in leak respiration. One of the main drivers of leak respiration is UCP1 (58) which uncouples ATP production from the electron transport chain and generates heat. In this study, Western blotting on iWAT protein lysates indicated an increase of Ucp1 expression in Sult1a1 KO mice. To clarify if changes in mitochondrial content contribute to increased respiratory capacity of Sult1a1 KO iWAT adipocytes, protein expression of VDAC, a protein of the mitochondrial membrane was quantified. VDAC was increased in adipocytes from the iWAT of Sult1a1 KO mice suggesting increased mitochondrial content. Together, elevated leak respiration with Ucp1 expression and increased mitochondrial content indicate the development of beige/brite adipocytes in white adipose tissue of Sult1a1 KO mice.

The presence of beige/brite adipocytes in white adipose tissue is known as browning and has gained attention for its potential to improve metabolic health by triggering an energy expending futile cycle mediated by Ucp1. Interestingly, increased futile cycling, specifically lipid futile cycling, was proposed as a mechanism to increase energy expenditure in CT humans (7). The observation of increased futile cycling in CT humans and Sult1a1 KO mice suggest that futile cycling may play an important role in resistance to weight gain.

Adipose tissue browning has been linked to increased EE and improvements in glucose/lipid homeostasis (59). In this study, adipose tissue browning was not linked to increased EE or changes in glucose homeostasis in mice on a standard diet. Differences in body composition could mask the effect of adipose tissue browning on EE of Sult1a1 KO mice. A recent publication by Mina and colleagues (2018) noted that the ANCOVA method can be overly restrictive in experiments involving brown adipose tissue (BAT) where differential interactions are observed between mass and EE. The publication recommends that when differential interactions are observed, the groups should be corrected independently rather than applying one correction to both groups, as done in the ANCOVA method. Mina and colleagues suggest that the differential interactions observed in BAT studies may arise from the fact that when EE is adjusted to lean mass, the contribution of BAT is not accounted for. Extending these observations to this study where WAT browning is implicated rather than BAT activation, the effect of WAT browning on EE could be masked as it is not accounted for in the EE adjustment. To account for the contribution of WAT browning towards EE, a future experiment could quantify adipose tissue browning in WT and Sult1a1 KO mice by measuring expression of beige adipocyte specific markers like Tmem26, Cd137, and Tbx1 (60). Future analysis of the EE data should correct each group independently using ‘ANCOVA for non-parallel slopes’ as recommended by Mina and colleagues (2018).

The results of this study show that glucose homeostasis does not differ between WT and Sult1a1 KO mice on a standard diet. In absolute terms, Sult1a1 KO mice have significantly less lean and fat mass however when body composition is adjusted for body size differences using ANCOVA, Sult1a1 KO mice have significantly less lean mass (≈ 8% decrease) and a significant increase in fat mass (≈ 40% increase). The glycaemia of WT and Sult1a1 KO mice on a standard diet is similar despite a relative reduction in lean

mass and relative increase in fat mass suggesting that adipose tissue contributes towards maintaining glucose homeostasis which is surprising since fat mass is correlated with increased risk of diabetes and insulin resistance (47). One possible mechanism that prevents the Sult1a1 KO mice from developing diabetes and insulin resistance despite elevated fat mass is increased oxidation of glucose driven by increased Ucp1 expression.

In this study, adipose tissue browning was specific to the inguinal depot of Sult1a1 KO mice. In the visceral depot, leak respiration was similar between the genotypes indicating that adipose tissue browning does not occur in the eWAT (visceral fat) of WT or Sult1a1 KO mice. This result was anticipated as adipose tissue browning is depot specific and in mice, the inguinal depot has the highest capacity for browning while the eWAT depot is browning resistant (61). An aspect that should be further investigated is Sult1a1 expression in different adipose tissue depots and if higher Sult1a1 expression is linked with increased Ucp1 expression. A future experiment could check if overexpression of Sult1a1 in the eWAT depot increases Ucp1 expression.

Another aspect that would be interesting to investigate are local hormonal changes in the adipose tissue depots of WT and Sult1a1 KO mice. Adipose tissue browning is triggered by hormones such as catecholamines (59) and thyroid hormone (62) which both contain phenolic rings with a hydroxyl group, a moiety that is prone to sulfonation. Loss of Sult1a1 may reduce sulfonation of catecholamines and/or thyroid hormone and increase their local concentration in tissues to promote adipose tissue browning.

Another aspect to consider is the contribution of inter-organ cross talk towards adipose tissue browning. For example, fibroblast growth factor 21 (FGF21) is a hormone secreted by the liver which mediates adipose tissue browning (63) and as Sult1a1 is abundantly expressed in the liver, loss of Sult1a1 may trigger pathways in the liver that modulate FGF21 expression. To test this hypothesis, a future experiment could measure FGF21 in the plasma collected from WT and Sult1a1 KO mice. Transcriptomics might also provide additional insight on changes within peripheral tissues that might influence adipose tissue browning.

Characterization of Sult1a1 KO mice on a HFD

Weight matched WT and Sult1a1 KO mice were placed on a HFD and body weight was tracked for 13-weeks. In this study, Sult1a1 KO mice on a HFD are resistant to weight gain. To determine if the resistance to weight gain could offer protection from the co-morbidities associated with diet-induced obesity, glycemia was characterized. WT and Sult1a1 KO mice have similar glycemia however Sult1a1 KO mice have reduced fasting plasma insulin levels suggesting that Sult1a1 KO mice have preserved insulin sensitivity. A similar phenotype was observed in genetically obese mice prone to adipose tissue browning through over expression of Prdm16 in adipose tissue. On a HFD, adipose tissue specific expression of Prdm16 increases browning and improves insulin sensitivity (64). This study assessed adipose tissue browning in mice on a standard diet only. Future experiments should quantify adipose tissue browning in mice on a HFD to determine if the improvement in glucose sensitivity observed in Sult1a1 KO mice on a HFD is through increased glucose oxidation mediated by Ucp1.

In this study, Sult1a1 KO mice on a HFD had preserved insulin sensitivity without changes in total fat mass or visceral fat pad mass. This observation was interesting as insulin resistance is positively correlated with fat mass and visceral fat (47). To investigate this further, sections of the eWAT visceral depot were stained with H & E to gain insight into changes in adipose tissue morphology. Histology on the eWAT sections from mice on a HFD indicated increased immune cell infiltration by the presence of neutrophils and macrophages in WT eWAT sections. Inflammation in the eWAT was associated with collagen streaks in WT mice. In Sult1a1 KO mice, immune cells and collagen deposits were less present in the eWAT indicating protection from inflammation and adipose tissue fibrosis.

To gain further insight into changes within the adipose tissue, transcriptomics on primary adipocytes isolated from the stromal vascular fraction of WT and Sult1a1 KO iWAT on a standard chow diet was performed. The pathway analysis identified a downregulation of the complement and acute phase response signaling in primary adipocytes of Sult1a1 KO mice. Transcripts common to the complement and acute phase response signaling pathways were C1R, C2 and C3. C1R, C2 and C3 are proteins of the complement cascade which when activated stimulate and recruit phagocytes as well as trigger formation of the membrane attack complex. Activation of the complement system and acute phase response signalling are

proinflammatory pathways. Additionally, the dataset also showed a downregulation of LBP which binds LPS. Obesity is associated with increased plasma LPS which is derived from the gut and activates proinflammatory pathways (48). In summary, C1R, C2, C3 and LBP were significantly downregulated in the primary cells of Sult1a1 KO mice indicating a reduction in the expression of proinflammatory pathways. Transcriptomics comparing normal body weight controls and CT adipose tissue showed a similar downregulation of proinflammatory pathways in CT individuals (7).

Another pathway identified in the analysis was the atherosclerosis signaling pathway. Annotated to this pathway was the COL1A1 transcript which was upregulated in the primary adipocytes of Sult1a1 KO mice. On a HFD, Sult1a1 KO mice had fewer collagen streaks in their adipose tissue. Together this information suggests that there are changes in the extracellular matrix (ECM) of adipose tissue from Sult1a1 KO mice. Since disulfide bridges are a structural component of the collagens, loss of Sult1a1 could influence the structure of the ECM by increasing the availability of sulfur through reduced demand for PAPS, the sulfur donor for the Sult1a1 enzyme. The ECM of adipose tissue from WT and Sult1a1 KO mice could be compared in future experiments to provide insight on changes in composition which could be protective against diet induced obesity. The expression of collagen VI in WT and Sult1a1 adipose tissue would be particularly interesting as collagen VI is associated with obesity in humans (65) and mice (66).

The effect of Sult1a1 deletion on the liver could be further characterized in future experiments as reduced liver mass was observed in Sult1a1 KO mice on a HFD. The reduced liver mass observed in the Sult1a1 KO mice could be due to reduced lipid accumulation and reduced fibrosis which would indicate protection from NAFLD, a complication of obesity (50). In future experiments, the TG content of the liver tissue could be measured to determine if loss of Sult1a1 reduces hepatic triglyceride content and offers protection from NAFLD. NAFLD is associated with increased DNL through upregulation of the transcription factors sterol regulatory element-binding protein 1 (SREBP1) and carbohydrate-responsive element-binding protein (ChREBP). Future experiments could quantify expression of SREBP1 and ChREBP to check if deletion of Sult1a1 is associated with reduced DNL. To quantify fibrosis, future experiments could measure collagen mRNA expression, perform SR staining which binds to collagen I, II and III (49) and measure collagen content.

Molecular mechanisms underlying the Sult1a1 KO mouse phenotype

To gain insight into the mechanisms driving the Sult1a1 phenotype transcriptomics was performed on the SGBS cell line, a model for human adipocytes (51), and primary mouse adipocytes. These datasets compared the transcriptome of WT and SULT1A1 knockdown adipocytes and WT and Sult1a1 KO primary adipocytes. Downregulation of the LXR/RXR signaling pathway was identified in both the human SGBS cell line and the primary mouse adipocyte datasets and it was speculated that loss of Sult1a1 downregulates the LXR/RXR signaling pathway. Additionally, in the SGBS dataset, the NR1H3 transcript/LXRα receptor was downregulated in SULT1A1 knockdown adipocytes.

Substrates for NR1H3, the transcript which codes for the LXRα receptor, are oxysterols which are typically sulfonated by the SULT2 family. Sulfonated oxysterols are reported to antagonize the LXRα receptor (52). A previous study reported that LXRα (NR1H3) acts as a transcriptional repressor of Ucp1 by binding directly to elements within the Ucp1 enhancer region. LXRα KO mice are lean and have increased Ucp1 expression in white adipose tissue (67). It was hypothesized that changes in oxysterol sulfonation decrease LXRα activity which removes the 'negative break' on Ucp1 thereby increasing its expression in WAT. To test this hypothesis, the affinity of SULT1A1 towards oxysterols was measured using a radiochemical assay to check if SULT1A1 directly contributes towards changes in oxysterol sulfonation.

In this study, the four oxysterols tested were not substrates for SULT1A1 suggesting that in mice Sult1a1 does not directly contribute to oxysterols sulfonation. One possibility is that loss of Sult1a1 induces compensatory mechanisms which increase the expression of SULT family members. Deletion of of Sult1a1 could increase the basal expression of the Sult2 family in adipose tissue which in turn increases the production of sulfonated oxysterols which antagonize the LXRα receptor de-repressing Ucp1 transcription resulting in Ucp1 expression in WAT. To investigate this further, future experiments should quantify expression of the Sult family of enzymes in the inguinal adipose tissue of WT and Sult1a1 KO mice to check for compensation by Sult family enzymes.

In summary, the molecular mechanism driving adipose tissue browning in the Sult1a1 KO mice remains unclear. Further studies to clarify the role of Sult2 compensation, catecholamines, thyroid hormone and the

contribution of tissues such as liver might provide mechanistic insight into the adipose tissue browning phenotype observed in Sult1a1 KO mice.

Metabolism of Sult1a1 substrates in Sult1a1 KO mice

To validate the Sult1a1 KO mouse model, WT and Sult1a1 KO mice were treated with a known Sult1a1 substrate. The substrate chosen was resveratrol as it is a phenolic molecule whose effects and kinetics are well described (68,69). When Sult1a1 KO mice are treated with resveratrol, increased accretion of resveratrol was observed in all the tissues investigated demonstrating that blocking Sult1a1 could be a method to increase bioavailability. A similar rodent study showed that blocking Ugt1a1, an enzyme that functions similar to Sult1a1 but adds glucuronic acid rather than sulfonate to molecules, with a natural inhibitor (piperine, a molecule present in black pepper) increased the bioavailability of resveratrol (70). Future studies could test if natural inhibitors of Sult1a1 improve the bioavailability of molecules that are sulfonated by dosing mice with natural Sult1a1 inhibitors and resveratrol (or another similar bioactive molecule).

An unanticipated result of this experiment was the presence of resveratrol sulfate metabolites in the tissue of Sult1a1 KO mice which indicated that there are compensatory mechanisms for the loss of Sult1a1. To investigate this further, Sult expression in the liver of WT and Sult1a1 KO mice was measured. With resveratrol treatment there was an induction of Sult5a1 expression suggesting that Sult5a1 compensates for the loss of Sult1a1. Without substrate (vehicle treated mice), Sult1a1 KO mice basally express more Sult1b1 in the liver. Dosing with resveratrol did not upregulate the expression of Sult1b1 indicating that resveratrol may not be a substrate for Sult1b1. Together this experiment suggests that Sult5a1 compensates for sulfonation of exogenous substrates while Sult1b1 may compensate for sulfonation of endogenous substrates. In mice, Sult1b1 has a high affinity towards dopamine (71). If Sult1b1 in the liver compensates for the loss of Sult1a1, this may result in reduced dopamine sulfonation, an aspect that could be explored in future studies.

In the liver, UHPLC-UV analysis of the metabolites indicated that there was a tendency towards increased resveratrol accretion in the liver, but similar levels of sulfated metabolites suggesting that the liver has mechanisms to compensate for loss of Sult1a1 by upregulating Sult5a1 expression. One of the concerns with Sult1a1 inhibition is that blockade of the Sult1a1 enzyme in the liver will reduce the metabolism of xenobiotics. This study demonstrates that resveratrol is still metabolized and that the liver can compensate for loss of Sult1a1 by upregulating Sult5a1 expression. Some tissues may not compensate as efficiently the liver for the loss of Sult1a1 which could explain the net increase in resveratrol accretion observed. Additional experiments are needed to understand Sult1a1 compensation in tissues like the kidney and colon which contribute to the pool of resveratrol metabolites. Understanding Sult1a1 compensation could help better target accretion in specific tissues. For example, the liver has a different Sult expression profile from the adipose tissue which expresses Sult1a1, Sulte1e1 and Sult5a1. The liver does not express Sult1e1 nor does it upregulate expression basally or in the presence of substrate. To increase the accretion of bioactives in the adipose tissue a Sult1a1 inhibitor could be paired with a bioactive that is not a substrate for Sult1e1 to ensure accretion and action in the adipose tissue. Additional experiments are needed to investigate compensatory mechanisms in the adipose tissue of Sult1a1 KO mice.

5. Conclusion

This thesis aimed to determine if SULT1A1 contributes to the constitutionally thin phenotype. To investigate the role of SULT1A1 in adipose tissue function and energy metabolism, a whole-body Sult1a1 KO mouse was characterized on a standard diet and a HFD.

Sult1a1 KO mice recapitulate features of the CT human phenotype (**Table 5**). CT humans and Sult1a1 KO mice have in common that they have a low body weight in comparison to their respective controls. On a HFD both the CT and Sult1a1 KO mice are resistant to weight gain. Increased futile cycling is implicated in both CT and Sult1a1 KO mice with differences in the molecular mechanism underlying the phenotype. In CT humans the proposed mechanism is increased lipid futile cycling while the results of this study suggest that futile cycling in Sult1a1 KO mice is mediated through Ucp1. Absolute fat mass is reduced in CT individuals and Sult1a1 KO mice. When fat mass is adjusted to body weight, CT humans have reduced fat mass relative to body mass while Sult1a1 KO mice have increased fat mass in relative terms an aspect that should be addressed in future studies. In common to both CT and Sult1a1 KO mice is reduced adipose tissue inflammation. The data from thesis indicates that on a standard diet and a HFD Sult1a1 KO mice are protected from adipose tissue inflammation which is a hallmark of insulin resistance. In comparison to normal weight controls, adipocyte size was reduced in CT individuals. Though the size of Sult1a1 KO adipocytes has not been quantified, the preserved insulin sensitivity and reduced inflammation observed in Sult1a1 KO mice suggests that adipocyte size may be reduced in Sult1a1 KO mice on a standard and HFD. CT individuals and normal weight human controls had similar leak respiration while leak respiration was elevated in Sult1a1 KO mice in comparison to WT controls. Increased leak respiration aligns with the observation of increased Ucp1 expression in the subcutaneous fat of Sult1a1 KO mice. In contrast to Sult1a1 KO mice, CT humans do not express UCP1 in their subcutaneous adipose tissue. Both CT and Sult1a1 KO mice have increased mitochondrial content in their adipose tissue which was linked to functional changes in mitochondrial biology.

In summary, this study demonstrates that Sult1a1 KO mice mirror key features of the CT phenotype such as low body weight and resistance to weight gain during overfeeding. A clinical trial investigating CT individuals did not observe differences in leak respiration or UCP1 expression indicating that adipose tissue browning is not implicated in the CT phenotype. Sult1a1 KO mice have increased leak respiration in their subcutaneous adipose tissue depot accompanied by Ucp1 expression suggesting that adipose tissue browning is unique to Sult1a1 KO mice and thus a differentiating characteristic of the Sult1a1 KO and CT phenotype. This thesis is the first to identify a role for Sult1a1 in adipose tissue browning and contributes towards understanding adipose tissue browning which has anti-obesity therapeutic potential.

Table 5: Comparison of CT humans and Sult1a1 KO mice

Feature	**CT humans**	**Sult1a1 KO mice**
Body weight	Low	Low
Resistance to weight gain on HFD	Yes	Yes
Futile cycling	Yes, via increased futile lipid cycling	Yes, via increased Ucp1
Absolute fat mass	Reduced	Reduced
Relative fat mass	Reduced	Increased
Adipose tissue inflammation	Reduced	Reduced
Adipocyte size	Reduced	Not yet characterized
UCP1 expression	Absent in subcutaneous fat	Present in subcutaneous fat
Leak respiration	Similar between CT and controls	Increased leak respiration
Mitochondrial content	Increased	Increased

6. References

1. Blüher M. Obesity: global epidemiology and pathogenesis. Vol. 15, Nature Reviews Endocrinology. Nature Publishing Group; 2019. p. 288–98.

2. Gray DS, Fujioka K. Use of relative weight and body mass index for the determination of adiposity. J Clin Epidemiol. 1991;44(6):21.

3. Khan SS, Ning H, Wilkins JT, Allen N, Carnethon M, Berry JD, et al. Association of body mass index with lifetime risk of cardiovascular disease and compression of morbidity. JAMA Cardiol. 2018 Apr 1;3(4):280–7.

4. World Health Organization. Obesity and overweight [Internet]. Obesity and overweight. 2020 [cited 2020 Apr 1]. Available from: https://www.who.int/news-room/fact-sheets/detail/obesity-and-overweight

5. Kelly T, Yang W, Chen CS, Reynolds K, He J. Global burden of obesity in 2005 and projections to 2030. Int J Obes. 2008;32(9):1431–7.

6. Orthofer M, Valsesia A, Mägi R, Wang QP, Kaczanowska J, Kozieradzki I, et al. Identification of ALK in Thinness. Cell. 2020;181(6):1246-1262.e22.

7. Ling Y, Carayol J, Galusca B, Canto C, Montaurier C, Matone A, et al. Persistent low body weight in humans is associated with higher mitochondrial activity in white adipose tissue. Am J Clin Nutr. 2019 Sep 1;110(3):605–16.

8. Riveros-McKay F, Mistry V, Bounds R, Hendricks A, Keogh JM, Thomas H, et al. Genetic architecture of human thinness compared to severe obesity. PLoS Genet. 2019;15(1):1–25.

9. Morton NM, Beltram J, Carter RN, Michailidou Z, Gorjanc G, McFadden C, et al. Genetic identification of thiosulfate sulfurtransferase as an adipocyte-expressed antidiabetic target in mice selected for leanness. Nat Med. 2016;22(7):771–9.

10. Germain N, Galusca B, Caron-Dorval D, Martin JF, Pujos-Guillot E, Boirie Y, et al. Specific appetite, energetic and metabolomics responses to fat overfeeding in resistant-to-bodyweight-gain constitutional thinness. Nutr Diabetes. 2014;4.

11. Jéquier E, Tappy L. Regulation of body weight in humans. Physiol Rev. 1999;79(2):451–80.

12. Gamage N, Barnett A, Hempel N, Duggleby RG, Windmill KF, Martin JL, et al. Human sulfotransferases and their role in chemical metabolism. Vol. 90, Toxicological Sciences. 2006. p. 5–22.

13. Speliotes EK, Willer CJ, Berndt SI, Monda KL, Thorleifsson G, Jackson AU, et al. Association analyses of 249,796 individuals reveal 18 new loci associated with body mass index. Nat Genet. 2010;42(11):937–48.

14. Glatt H. Sulfotransferases in the bioactivation of xenobiotics [Internet]. Vol. 129, Chemico-Biological Interactions. 2000. Available from: www.elsevier.com/locate/chembiont*

15. Monien BH, Herrmann K, Florian S, Glatt H. Metabolic activation of furfuryl alcohol: Formation of 2-methylfuranyl DNA adducts in Salmonella typhimurium strains expressing human sulfotransferase 1A1 and in FVB/N mice. Carcinogenesis. 2011;32(10):1533–9.

16. Herrmann K, Engst W, Meinl W, Florian S, Cartus AT, Schrenk D, et al. Formation of hepatic DNA adducts by methyleugenol in mouse models: Drastic decrease by Sult1a1 knockout and strong increase by transgenic human SULT1A1/2. Carcinogenesis. 2014;35(4):935–41.

17. Langford R, Hurrion E, Dawson PA. Genetics and pathophysiology of mammalian sulfate biology.

Vol. 44, Journal of Genetics and Genomics. Institute of Genetics and Developmental Biology; 2017. p. 7–20.

18. Coughtrie MWH. Function and organization of the human cytosolic sulfotransferase (SULT) family. Chem Biol Interact. 2016 Nov 25;259:2–7.

19. Marto N, Morello J, Monteiro E, Pereira S. Implications of sulfotransferase activity in interindividual variability in drug response clinical perspective on current knowledge. Drug Metab Rev. 2017;49(3):357–71.

20. Brix LA, Barnett AC, Duggleby RG, Leggett B, McManus ME. Analysis of the substrate specificity of human sulfotransferases SULT1A1 and SULT1A3: Site-directed mutagenesis and kinetic studies. Biochemistry. 1999 Aug 10;38(32):10474–9.

21. Hildebrandt MAT, Salavaggione OE, Martin YN, Flynn HC, Jalal S, Wieben ED, et al. Human SULT1A3 pharmacogenetics: Gene duplication and functional genomic studies. Biochem Biophys Res Commun. 2004 Sep 3;321(4):870–8.

22. Takahashi S, Sakakibara Y, Mishiro E, Kouriki H, Nobe R, Kurogi K, et al. Molecular Cloning, Expression and Characterization of A Novel Mouse SULT6 Cytosolic Sulfotransferase. J Biochem. 2009 Sep 1;146(3):399–405.

23. Halls C, Yu O. Potential for metabolic engineering of resveratrol biosynthesis. Vol. 26, Trends in Biotechnology. 2008. p. 77–81.

24. Burns J, Yokota T, Ashihara H, Lean MEJ, Crozier A. Plant foods and herbal sources of resveratrol. J Agric Food Chem. 2002;50(11):3337–40.

25. Britton RG, Kovoor C, Brown K. Direct molecular targets of resveratrol: identifying key interactions to unlock complex mechanisms. Ann N Y Acad Sci. 2015;1348(1):124–33.

26. Miksits M, Wlcek K, Svoboda M, Kunert O, Haslinger E, Thalhammer T, et al. Antitumor activity of resveratrol and its sulfated metabolites against human breast cancer cells. Planta Med. 2009;75(11):1227–30.

27. Menet MC, Marchal J, Dal-Pan A, Taghi M, Nivet-Antoine V, Dargère D, et al. Resveratrol metabolism in a non-human primate, the grey mouse lemur (Microcebus murinus), using ultra-high-performance liquid chromatography- quadrupole time of flight. PLoS One. 2014 Mar 24;9(3).

28. Ensembl. Transcript: SULT1A1-202 [Internet]. Transcript: SULT1A1-202. 2020 [cited 2020 Oct 5]. Available from: http://www.ensembl.org/Homo_sapiens/Transcript/Summary?db=core;g=ENSG00000196502;r=16:28605196-28623625;t=ENST00000350842

29. Riches Z, Stanley EL, Bloomer JC, Coughtrie MWH. Quantitative evaluation of the expression and activity of five major sulfotransferases (SULTs) in human tissues: The SULT “pie.” Drug Metab Dispos. 2009 Nov;37(11):2255–61.

30. BioGPS. SULT1A1 (sulfotransferase family 1A member 1). SULT1A1 (sulfotransferase family 1A member 1). 2020.

31. Ensembl. Transcript: Sult1a1-201. Transcript: Sult1a1-201. 2020.

32. UniProt. UniProtKB - P50225 (ST1A1_HUMAN). UniProtKB - P50225 (ST1A1_HUMAN). 2020.

33. UniProt. UniProtKB - P52840 (ST1A1_MOUSE). UniProtKB - P52840 (ST1A1_MOUSE). 2020.

34. BioGPS. Sulfotransferase family 1A, phenol-preferring, member 1 [Internet]. Sulfotransferase family 1A, phenol-preferring, member 1. 2020 [cited 2020 Sep 14]. Available from: http://biogps.org/#goto=genereport&id=20887

35. Alnouti Y, Klaassen CD. Tissue distribution and ontogeny of sulfotransferase enzymes in mice. Toxicol Sci. 2006 Oct;93(2):242–55.

36. Zhang F, Hao G, Shao M, Nham K, An Y, Wang Q, et al. An Adipose Tissue Atlas: An Image-Guided Identification of Human-like BAT and Beige Depots in Rodents. Cell Metab. 2018 Jan 9;27(1):252-262.e3.

37. Scheja L, Heeren J. The endocrine function of adipose tissues in health and cardiometabolic disease. Vol. 15, Nature Reviews Endocrinology. Nature Publishing Group; 2019. p. 507–24.

38. Rousset S, Alves-Guerra M-C, Mozo J, Miroux B, Cassard-Doulcier A-M, Dé Ric Bouillaud F, et al. The Biology of Mitochondrial Uncoupling Proteins. 2004.

39. Chouchani ET, Kajimura S. Metabolic adaptation and maladaptation in adipose tissue. Vol. 1, Nature Metabolism. Nature Research; 2019. p. 189–200.

40. Herrmann K, Engst W, Meinl W, Florian S, Cartus AT, Schrenk D, et al. Formation of hepatic DNA adducts by methyleugenol in mouse models: Drastic decrease by Sult1a1 knockout and strong increase by transgenic human SULT1A1/2. Carcinogenesis. 2014;35(4):935–41.

41. Virtue S, Vidal-Puig A. Assessment of brown adipose tissue function. Front Physiol. 2013;4.

42. Schöttl T, Kappler L, Fromme T, Klingenspor M. Limited OXPHOS capacity in white adipocytes is a hallmark of obesity in laboratory mice irrespective of the glucose tolerance status. Mol Metab. 2015 Sep 1;4(9):631–42.

43. Schöttl T, Kappler L, Braun K, Fromme T, Klingenspor M. Limited mitochondrial capacity of visceral versus subcutaneous white adipocytes in male C57BL/6N mice. Endocrinology. 2015 Mar 1;156(3):923–33.

44. Li Y, Bolze F, Fromme T, Klingenspor M. Intrinsic differences in BRITE adipogenesis of primary adipocytes from two different mouse strains. Biochim Biophys Acta - Mol Cell Biol Lipids [Internet]. 2014;1841(9):1345–52. Available from: http://dx.doi.org/10.1016/j.bbalip.2014.06.003

45. Hausman DB, Park HJ, Hausman GJ. Isolation and culture of preadipocytes from rodent white adipose tissue. Methods Mol Biol. 2008;456(1):201–19.

46. Ma F, Fuqua BK, Hasin Y, Yukhtman C, Vulpe CD, Lusis AJ, et al. A comparison between whole transcript and 3' RNA sequencing methods using Kapa and Lexogen library preparation methods 06 Biological Sciences 0604 Genetics. BMC Genomics. 2019;20(1):1–12.

47. Després J-P, Lemieux I. Abdominal obesity and metabolic syndrome. Nature. 2006;444:881–7.

48. Cani PD, Amar J, Iglesias MA, Poggi M, Knauf C, Bastelica D, et al. Metabolic endotoxemia initiates obesity and insulin resistance. Diabetes. 2007;56(7):1761–72.

49. Rittié L. Method for Picrosirius Red-Polarization Detection. Fibros Methods Protoc Methods Mol Biol. 2017;1627:395–407.

50. Brunt EM, Wong VWS, Nobili V, Day CP, Sookoian S, Maher JJ, et al. Nonalcoholic fatty liver disease. Nat Rev Dis Prim. 2015;1(December):1–22.

51. Fischer-Posovszky P, Newell FS, Wabitsch M, Tornqvist HE. Human SGBS cells - A unique tool for studies of human fat cell biology. Obes Facts. 2008;1(4):184–9.

52. Mutemberezi V, Guillemot-Legris O, Muccioli GG. Oxysterols: From cholesterol metabolites to key mediators. Prog Lipid Res [Internet]. 2016;64:152–69. Available from: http://dx.doi.org/10.1016/j.plipres.2016.09.002

53. Parra-Vargas M, Ramon-Krauel M, Lerin C, Jimenez-Chillaron JC. Size Does Matter: Litter Size Strongly Determines Adult Metabolism in Rodents. Cell Metab [Internet]. 2020;32(3):334–40.

Available from: https://doi.org/10.1016/j.cmet.2020.07.014

54. Speakman JR. Measuring energy metabolism in the mouse - theoretical, practical, and analytical considerations. Front Physiol. 2013;4 MAR(March):1–23.

55. Tschöp MH, Speakman JR, Arch JRS, Auwerx J, Brüning JC, Chan L, et al. A guide to analysis of mouse energy metabolism. Nat Methods. 2012;9(1):57–63.

56. Mina AI, LeClair RA, LeClair KB, Cohen DE, Lantier L, Banks AS. CalR: A Web-Based Analysis Tool for Indirect Calorimetry Experiments. Cell Metab [Internet]. 2018;28(4):656-666.e1. Available from: https://doi.org/10.1016/j.cmet.2018.06.019

57. Fernández-Verdejo R, Ravussin E, Speakman JR, Galgani JE. Progress and challenges in analyzing rodent energy expenditure. Nat Methods [Internet]. 2019;16(9):797–9. Available from: http://dx.doi.org/10.1038/s41592-019-0513-9

58. Jastroch M, Divakaruni AS, Mookerjee S, Treberg JR, Brand MD. Mitochondrial proton and electron leaks oxygen consumption and pH data. Essays Biochem . 2010;53–67.

59. Kajimura S, Spiegelman BM, Seale P. Brown and beige fat: Physiological roles beyond heat generation. Cell Metab [Internet]. 2015;22(4):546–59. Available from: http://dx.doi.org/10.1016/j.cmet.2015.09.007

60. Wu J, Boström P, Sparks LM, Ye L, Choi JH, Giang AH, et al. Beige adipocytes are a distinct type of thermogenic fat cell in mouse and human. Cell. 2012;150(2):366–76.

61. Ohno H, Shinoda K, Spiegelman BM, Kajimura S. PPARγ agonists induce a white-to-brown fat conversion through stabilization of PRDM16 protein. Cell Metab [Internet]. 2012;15(3):395–404. Available from: http://dx.doi.org/10.1016/j.cmet.2012.01.019

62. Senese R, Cioffi F, De Matteis R, Petito G, de Lange P, Silvestri E, et al. 3,5 Diiodo-l-Thyronine (T2) Promotes the Browning of White Adipose Tissue in High-Fat Diet-Induced Overweight Male Rats Housed at Thermoneutrality. Cells. 2019;8(3):256.

63. Fisher FF, Kleiner S, Douris N, Fox EC, Mepani RJ, Verdeguer F, et al. FGF21 regulates PGC-1α and browning of white adipose tissues in adaptive thermogenesis. Genes Dev. 2012;26(3):271–81.

64. Seale P, Conroe HM, Estall J, Kajimura S, Frontini A, Ishibashi J, et al. Prdm16 determines the thermogenic program of subcutaneous white adipose tissue in mice. J Clin Invest. 2011;121(1):96–105.

65. Pasarica M, Gowronska-Kozak B, Burk D, Remedios I, Hymel D, Gimble J, et al. Adipose tissue collagen VI in obesity. J Clin Endocrinol Metab. 2009;94(12):5155–62.

66. Khan T, Muise ES, Iyengar P, Wang Z V., Chandalia M, Abate N, et al. Metabolic Dysregulation and Adipose Tissue Fibrosis: Role of Collagen VI. Mol Cell Biol. 2009;29(6):1575–91.

67. Wang H, Zhang Y, Yehuda-Shnaidman E, Medvedev A V., Kumar N, Daniel KW, et al. Liver X Receptor α Is a Transcriptional Repressor of the Uncoupling Protein 1 Gene and the Brown Fat Phenotype. Mol Cell Biol. 2008;28(7):2187–200.

68. Sale S, Verschoyle RD, Boocock D, Jones DJL, Wilsher N, Ruparelia KC, et al. Pharmacokinetics in mice and growth-inhibitory properties of the putative cancer chemopreventive agent resveratrol and the synthetic analogue trans 3,4,5,4′-tetramethoxystilbene. Br J Cancer. 2004;90(3):736–44.

69. Menet MC, Cottart CH, Taghi M, Nivet-Antoine V, Dargère D, Vibert F, et al. Ultra high performance liquid chromatography-quadrupole-time of flight analysis for the identification and the determination of resveratrol and its metabolites in mouse plasma. Anal Chim Acta [Internet]. 2013;761:128–36. Available from: http://dx.doi.org/10.1016/j.aca.2012.11.048

70. Johnson JJ, Nihal M, Siddiqui I a, Scarlett CO, Howard H, Mukhtar H, et al. Enhancing the

bioavailability of resveratrol by combining it with piperine. Mol Nutr Food Res. 2012;55(8):1169–76.

71. Saeki Y, Sakakibara Y, Araki Y, Yanagisawa K, Suiko M, Nakajima H, et al. Molecular Cloning, Expression, and Characterization of a Novel Mouse Liver SULT1B1 Sulfotransferase1. Vol. 124, J. Biochem. 1998.

7. Supplementary Figures

Supplementary Figure 1

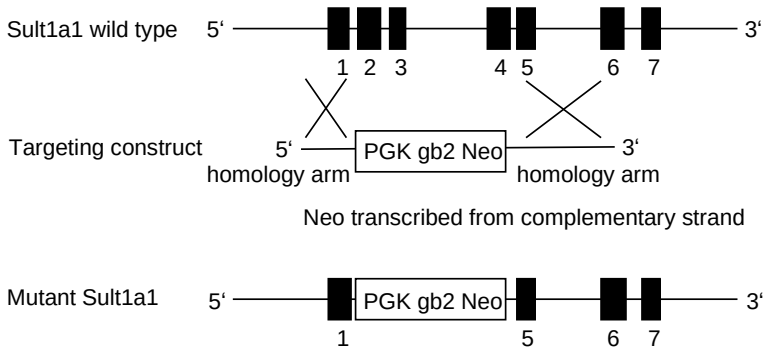

Supplementary Fig. 1: Targeting construct used to generate the Sult1a1 mutation. Targeting vector design provided by Walter Meinl at the DIfE.

Supplementary Figure 2

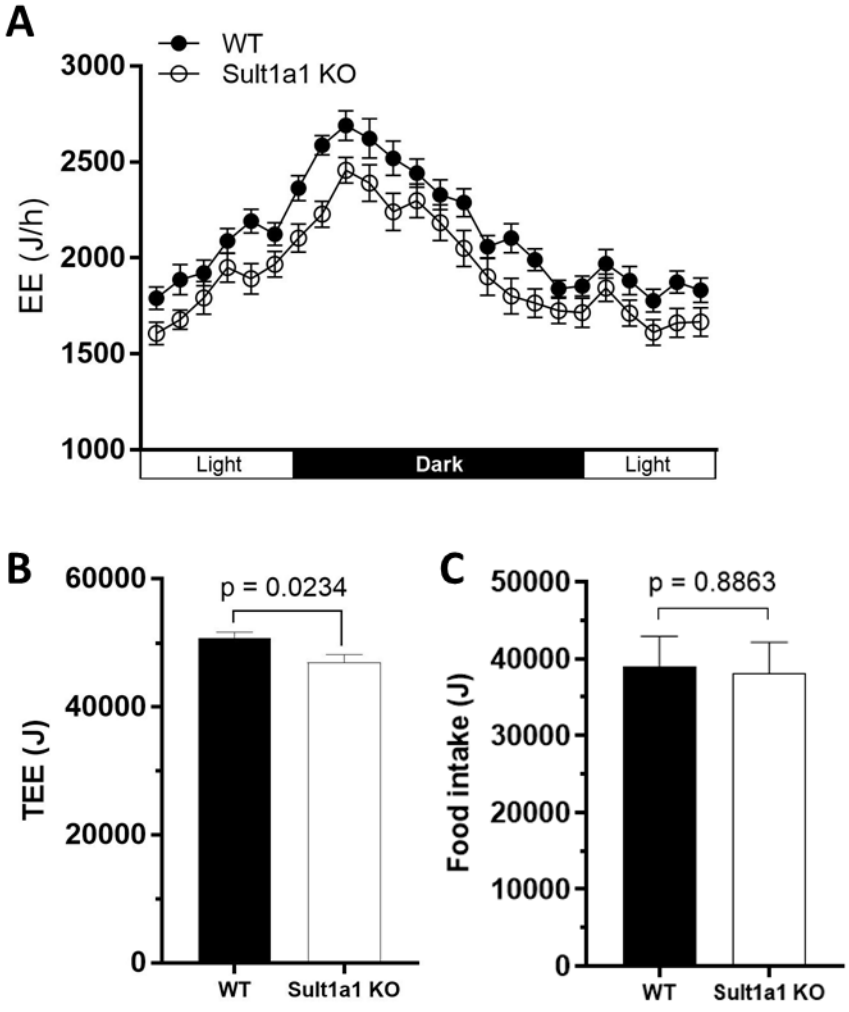

Supplementary Fig. 2: Energy balance of WT and Sult1a1 KO mice on a standard diet measured at 14-weeks old.

A. Unadjusted EE of WT and Sult1a1 KO mice housed in metabolic cages. Data represented as mean ± SEM. n = 13-15 mice per time point measured

B. The sum of the hourly EE shown in **Supplementary Fig. 2A**. TEE in units J and represented as mean ± SEM. n = 14-15 mice. p value was calculated using an unpaired Student's t test

C. 24-hour food intake of mice housed in metabolic cages at 14-weeks old. Food intake shown in units J for comparison to TEE. Data represented as mean ± SEM. n = 14-15 per genotype. p value was calculated using an unpaired Student's t test.

Supplementary Figure 3

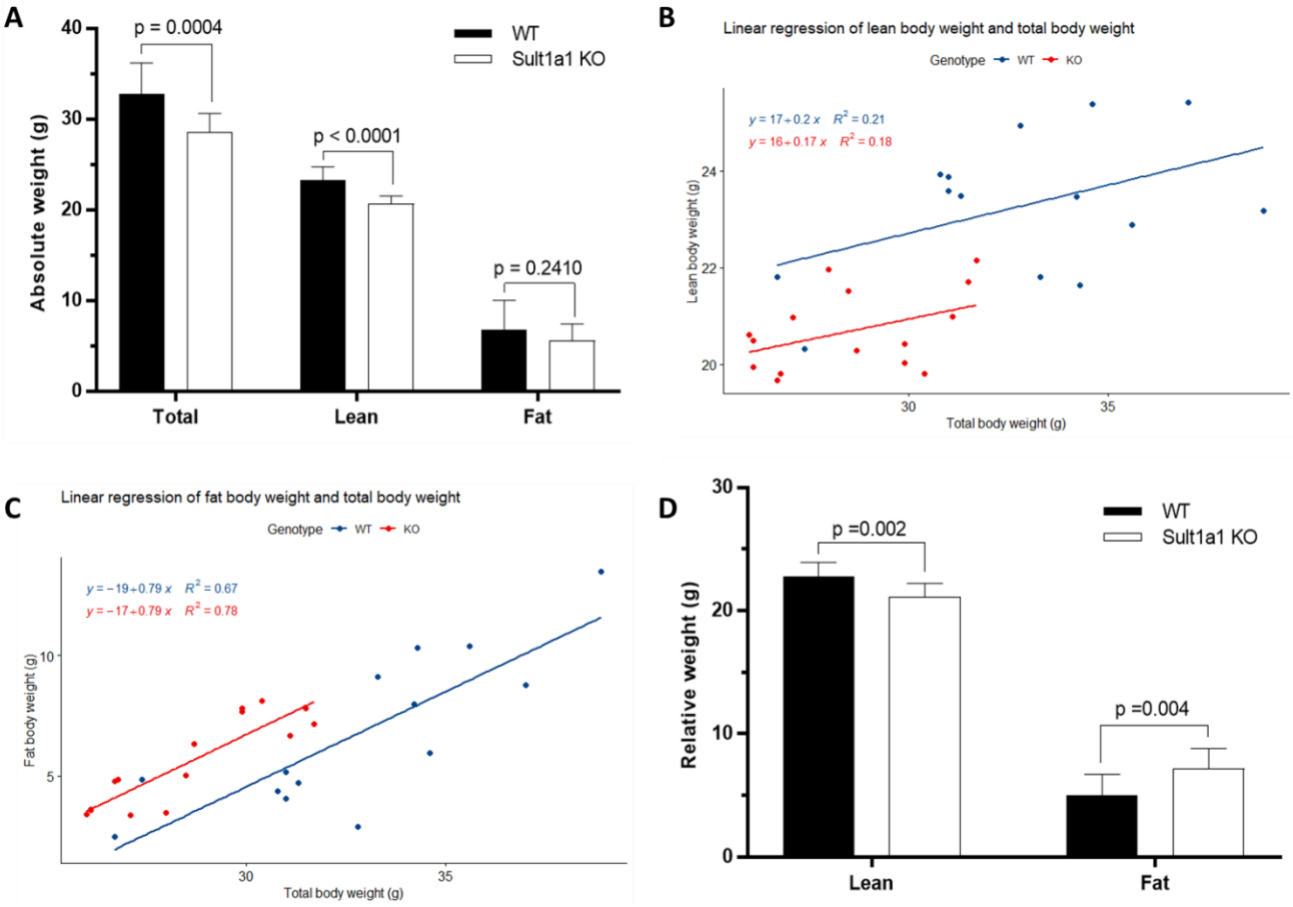

Supplementary Fig. 3: Body composition of WT and Sult1a1 KO mice on a standard diet at 14-weeks old. Body composition was measured directly after energy expenditure measurements. For WT, n = 14 and for Sult1a1 KO, n = 15.

- **A.** Absolute (unadjusted) body composition of Sult1a1 KO and WT mice. Sult1a1 KO mice have a statistically significant reduction in body weight and lean body weight and tend to have reduced fat weight. Data represented as mean ± SD. p values were calculated by using an unpaired Student's t test
- **B.** Linear regression plots of lean body weight (g) and total body weight (g) of WT (dark blue dots) and Sult1a1 KO (red dots) on a standard diet
- **C.** Linear regression plots of fat body weight (g) and total body weight (g) of WT (dark blue dots) and Sult1a1 KO (red dots) on a standard diet
- **D.** Relative body composition weights of Sult1a1 KO and WT mice. Body composition was adjusted for differences in body weight using ANCOVA. When adjusted for body weight, Sult1a1 KO mice have decreased lean weight and increased fat weight in comparison to WT mice. Data represented as mean ± SD. p values were calculated by using an unpaired Student's t test

Supplementary Figure 4

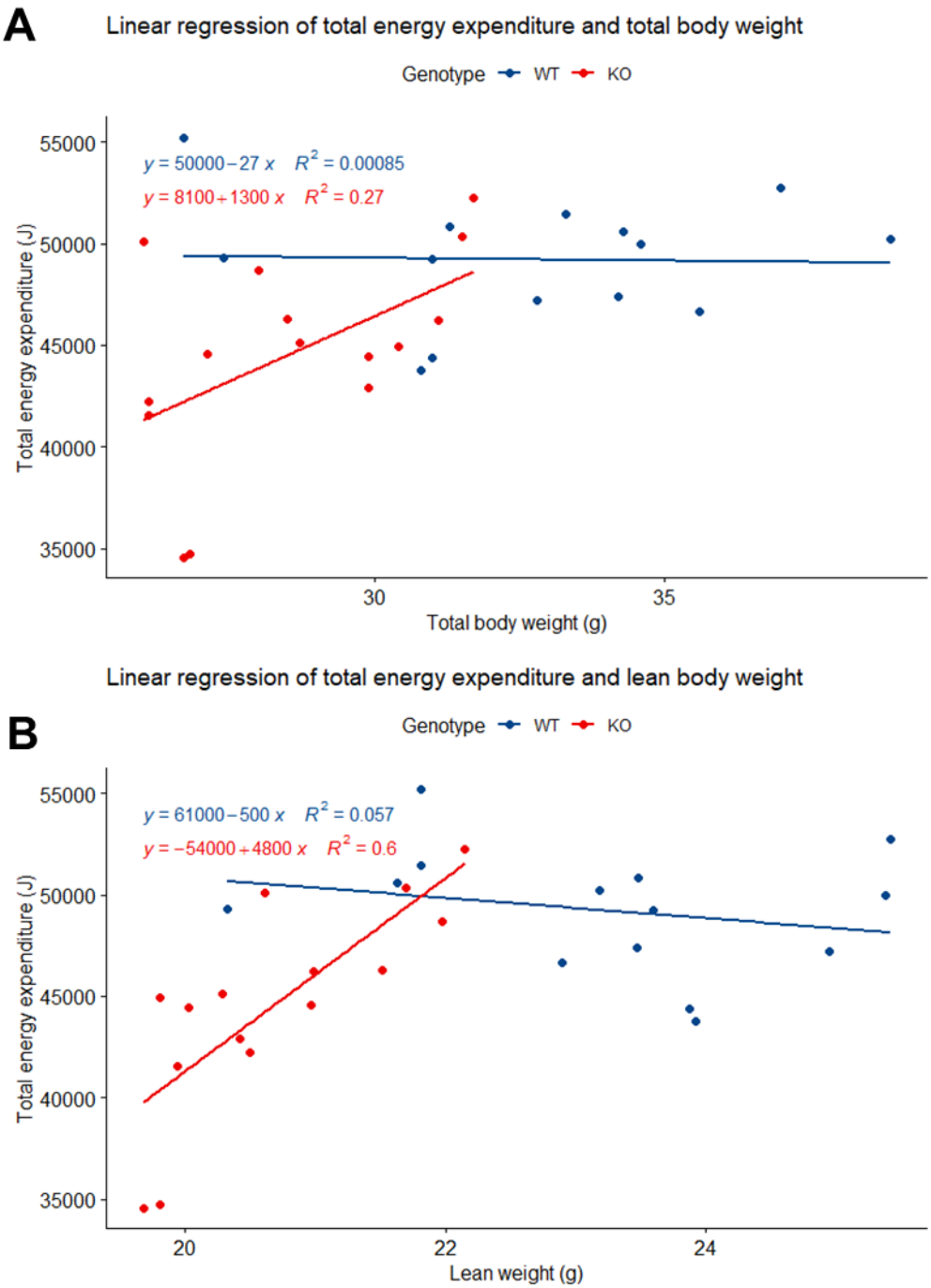

Supplementary Fig. 4: Linear regression plots of total energy expenditure and body composition. For WT, n = 14 and for Sult1a1 KO, n = 15.

- **A.** Regression plots of total energy expenditure (J) and lean body weight (g) of WT (dark blue dots) and Sult1a1 KO (red dots) on a standard diet
- **B.** Regression plots of total energy expenditure (J) and total body weight (g) of WT (dark blue dots) and Sult1a1 KO (red dots) on a standard diet

Supplementary Figure 5

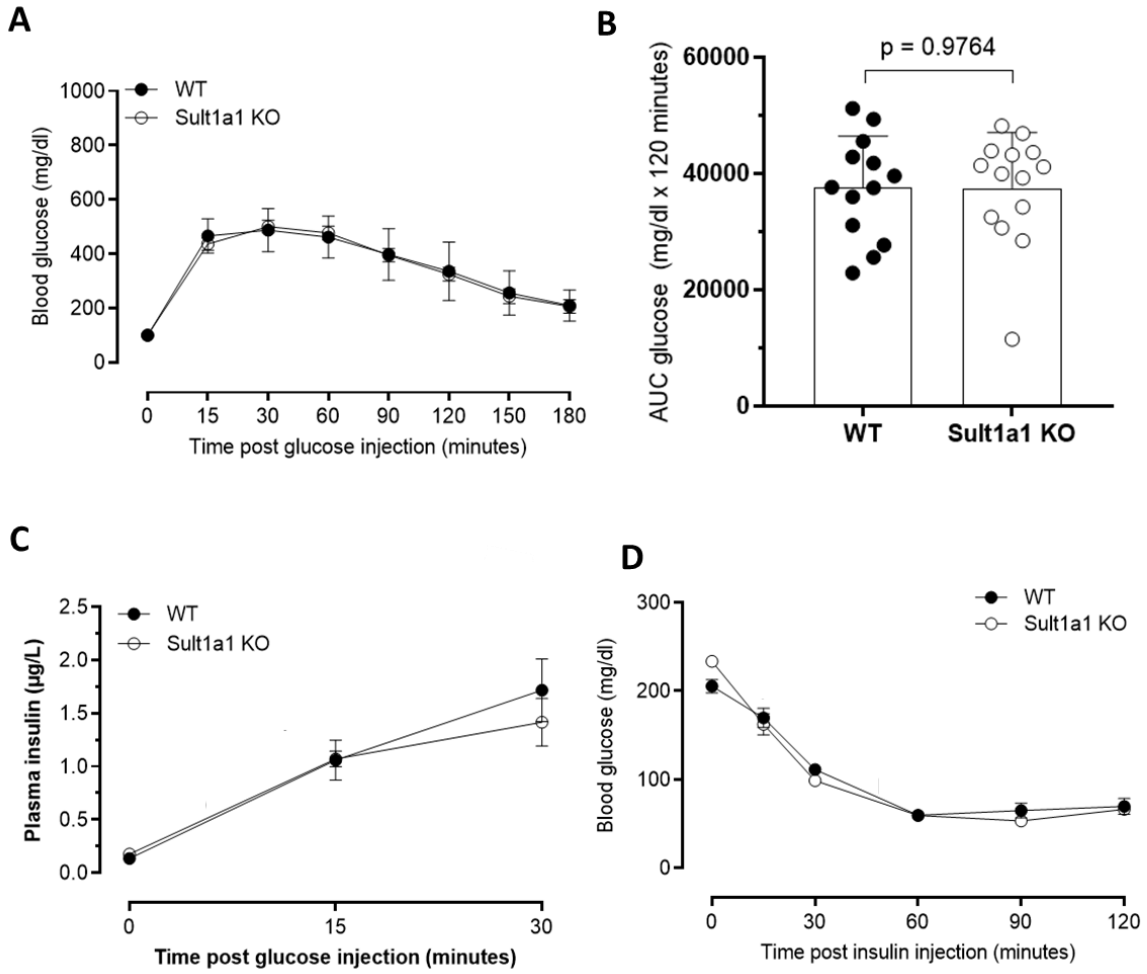

Supplementary Fig. 5: Glycaemia of Sult1a1 KO mice and WT mice on a standard diet. The IPGTT was performed on 14-week old mice and the ITT was performed 2 weeks later on the same mice.

A. Blood glucose concentration of WT and Sult1a1 KO mice following a glucose bolus administered via i.p. injection. n = 13-14 per genotype. Each time point represents the mean ± SD.

B. AUC glucose from 0 to 120 minutes from the time course shown in panel A. n = 13-14 per genotype. Data represented as mean ± SD. p value calculated using an unpaired Student's t test.

C. Insulin secretion during the IPGTT. n = 14-15 mice per genotype. Data represented as mean ± SD.

D. Blood glucose concentration of WT and Sult1a1 KO mice following an i.p. insulin injection. n = 7-13 mice per genotype. Each time point represents the mean ± SD.

Supplementary Figure 6

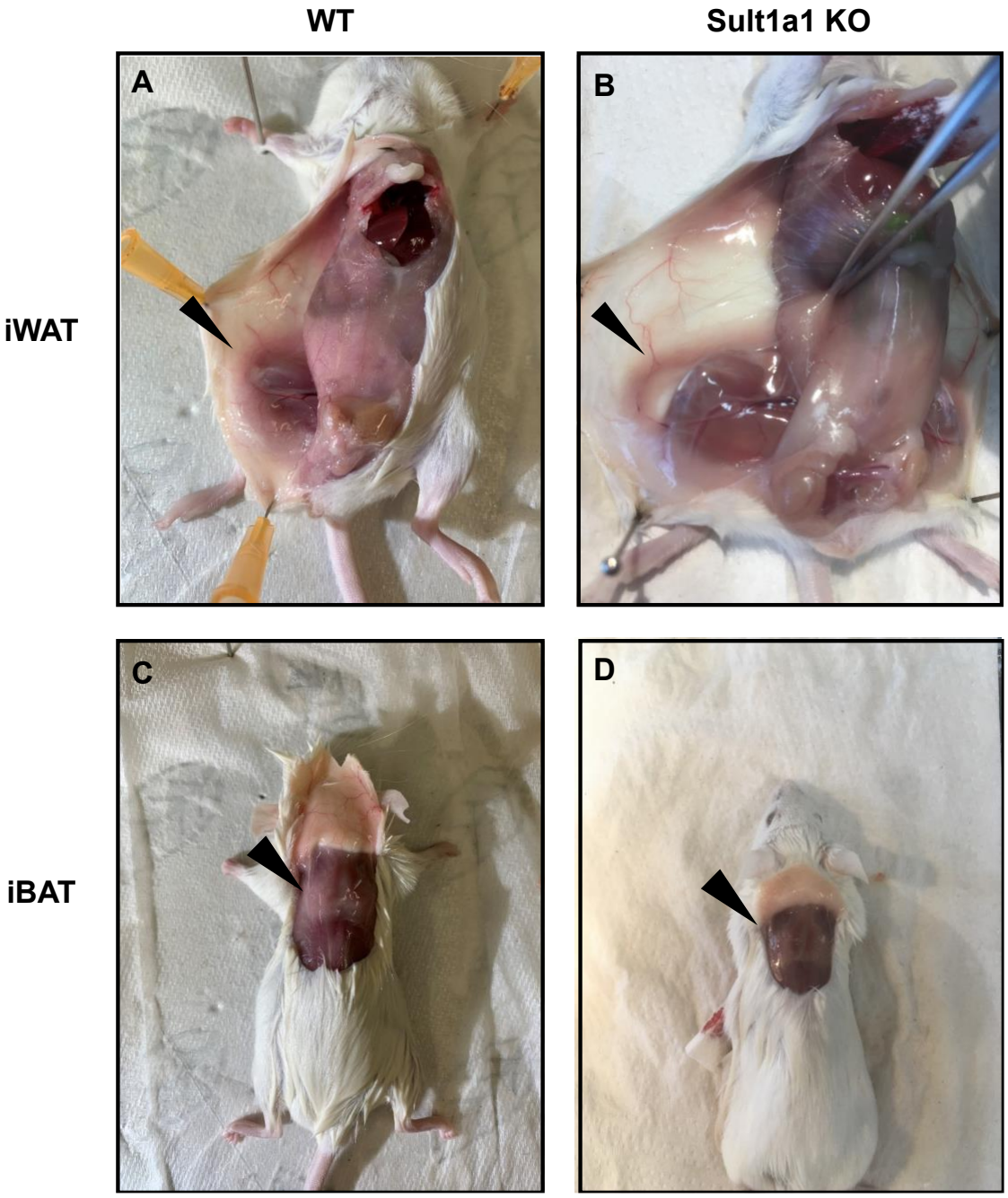

Supplementary Fig. 6: Images of WT and Sult1a1 KO adipose tissue depots. A. iWAT of a WT and **B.** Sult1a1 KO mouse. In panels A and B, arrowhead indicates the iWAT depot. **C.** iBAT of WT and **D.** Sult1a1 KO mouse. In panels C and D, arrowhead indicates the iBAT depot.

Supplementary Figure 7

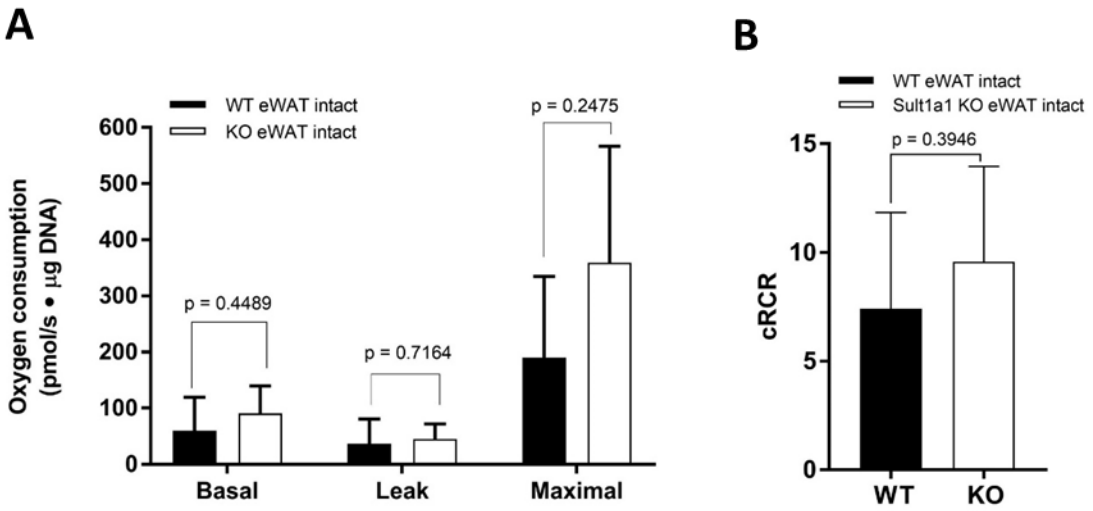

Supplementary Fig. 7. Respiratory capacity of intact eWAT adipocytes isolated from Sult1a1 KO and WT mice on a standard diet

A. Higher but not statistically significant increased respiratory capacity in adipocytes isolated from eWAT of Sult1a1 knockout mice (n = 3-4). Basal respiration was measured using pyruvate (5µM) and malate (5µM) as a substrates. Leak respiration was measured by inhibiting ATP synthase with oligomycin (2µg/ml). Titration of FCCP (0.5 µM steps) was used to determine maximal respiration. Non-mitochondrial respiration was measured by adding antimycin A (2.5 µM) and subtracted from all other respiratory states. Oxygen consumption was normalized by µg of DNA per chamber. Data represented as mean ± SEM. p values were calculated by using an unpaired Student's t test

B. No difference in mitochondrial integrity of intact eWAT from Sult1a1 KO and WT mice. The cellular respiratory control ratio (cRCR) was calculated by dividing maximal respiration by leak respiration. Data represented as mean ± SD. p values were calculated by using an unpaired Student's t test.

Supplementary Figure 8

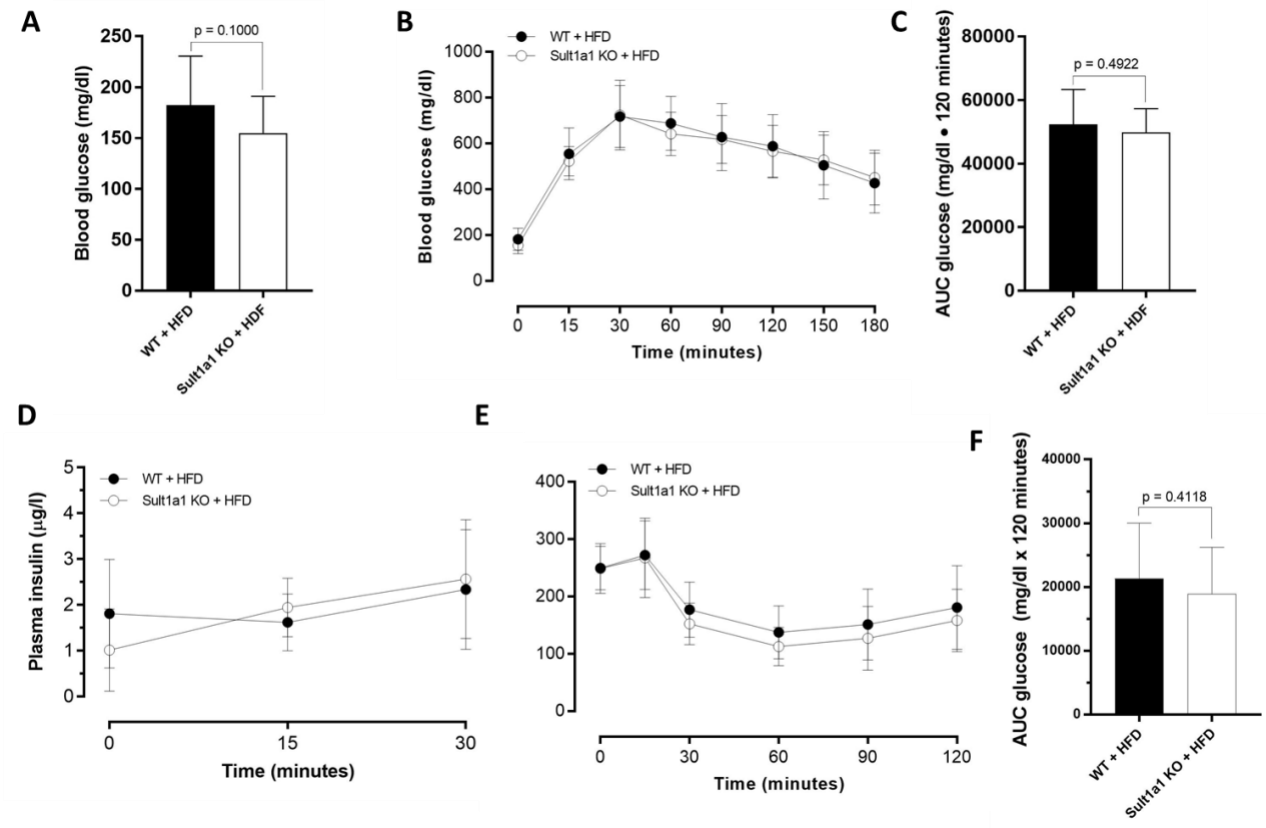

Supplementary Fig. 8: Glycaemia of Sult1a1 KO mice and WT mice on a high-fat diet (HFD). n = 14-15 per genotype. Data represented as mean ± SD. p values were calculated by using an unpaired Student's t test. Data from panel A to D was collected from mice on HFD for 9 weeks. Data from panel E and F was collected two weeks later (after 11 weeks on a HFD) from the same mice shown in panel A to D.

- **A.** Comparison of fasting blood glucose of Sult1a1 KO and WT mice on HFD for 9 weeks.
- **B.** Time course of blood glucose concentration during the glucose tolerance test (GTT). Glucose bolus dosed at 2 g/kg body weight and administered by intraperitoneal (ip) injection.
- **C.** AUC glucose from 0 to 120 minutes from the time course shown in panel B.
- **D.** Plasma insulin concentration during the GTT shown in panel B. At baseline (fasting), Sult1a1 KO had significantly reduced plasma insulin (p = 0.0453), bar chart show in main **Fig. 3B**. No significant difference between the genotypes 15 minutes post glucose injection (p = 0.1815) or 30 minutes post glucose injection (p = 0.6427).
- **E.** Time course of insulin tolerance test (ITT) from mice on a HFD for 11 weeks. Insulin was administered by ip injection at a dose of 1 IU/kg body weight.
- **F.** AUC glucose from 0 to 120 minutes from the time course shown in panel E

Supplementary Figure 9

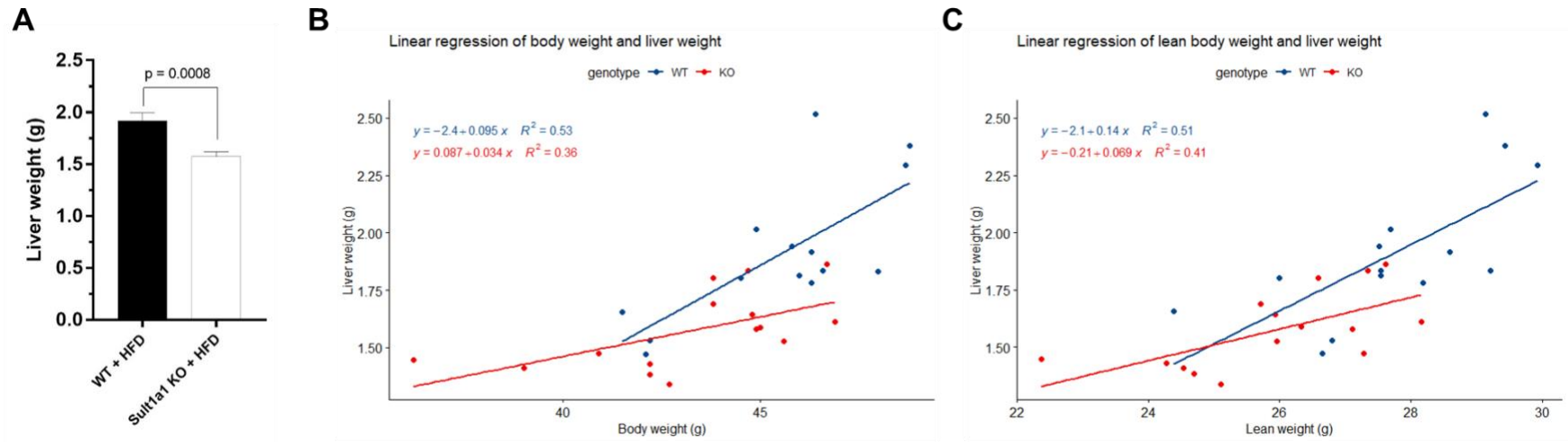

Supplementary Fig. 9: Sult1a1 KO mice have significantly smaller livers in comparison to WT control mice. For WT, n = 14 and for Sult1a1 KO, n = 15. Absolute (unadjusted) weight of liver collected from mice on a HFD for 13 weeks.

A. Liver weight of WT and Sult1a1 KO after 13-weeks on a HFD. p value was calculated using an unpaired Student's t test. Data represented as mean ± SEM

B. Regression plots of liver weight (g) and total body weight (g) of WT (dark blue dots) and Sult1a1 KO (red dots) on a HFD for 13-weeks

C. Regression plots of liver weight (g) and lean body weight (g) of WT (dark blue dots) and Sult1a1 KO (red dots) on a HFD for 13-weeks

Supplementary Figure 10

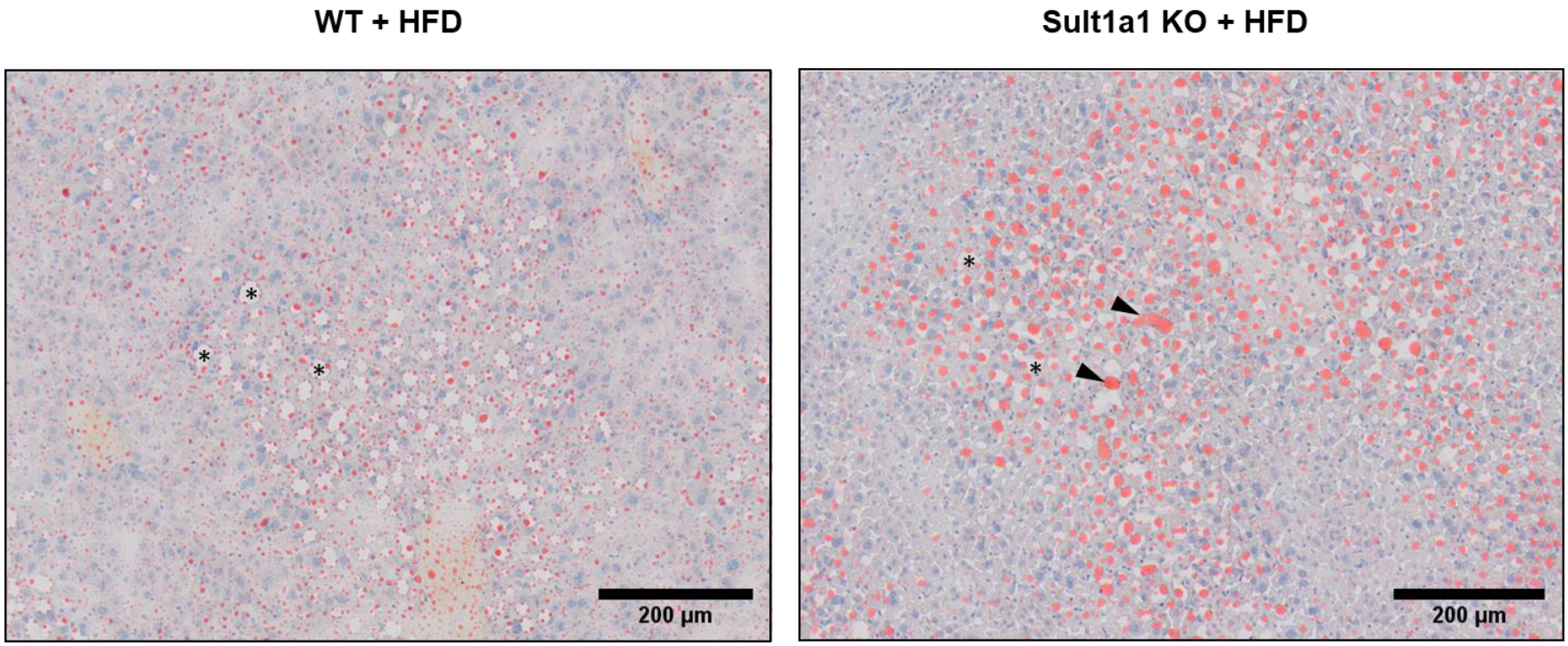

Supplementary Fig. 10: Liver sections stained with Oil Red O from mice on a high-fat diet (HFD). Representative image of a WT section (left) stars indicate partially stained lipid droplets. Representative image from liver of Sult1a1 KO mouse (right), stars indicate partially stained lipid droplets and arrowheads indicate areas of unspecific staining.

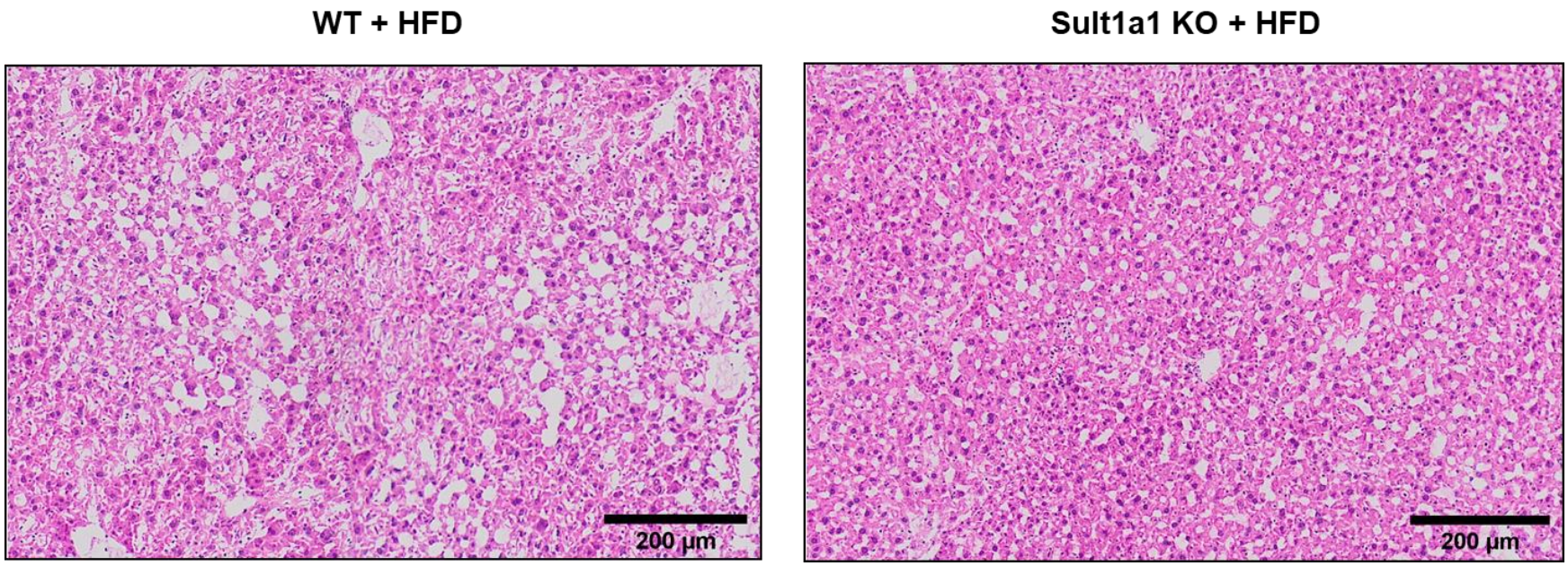

Supplementary Fig. 11: Liver sections from WT and Sult1a1 KO mice on a HFD stained with H&E. Representative images from WT liver (left) and Sult1a1 KO liver (right) stained with H&E

Supplementary Figure 12

A

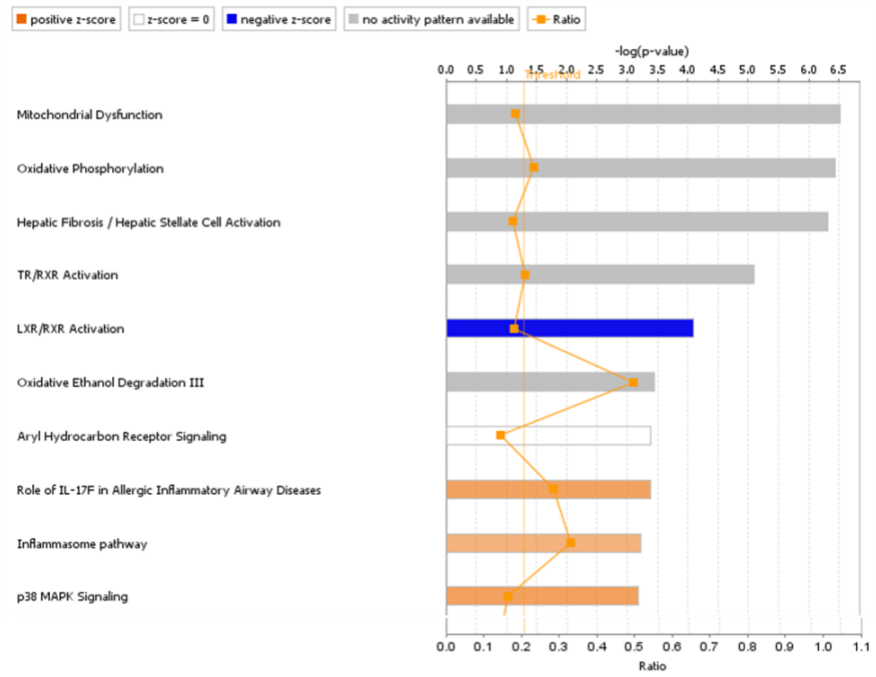

B

Symbol	Entrez Gene Name	Expression Value	
		Expr False Discovery	Expr Fold Change
CCL2	C-C motif chemokine ligand 2	1.28E-04	↑1.617
IL18	interleukin 18	9.17E-06	↑1.279
IL1B	interleukin 1 beta	9.19E-05	↓-1.405
IL1R1	interleukin 1 receptor type 1	4.30E-04	↑1.220
LDLR	low density lipoprotein	1.40E-03	↑1.255
LPL	lipoprotein lipase	1.56E-02	↓-1.267
NFKB1	nuclear factor kappa B subunit	5.81E-05	↑1.403
NR1H3	nuclear receptor subfamily 1	6.78E-04	↓-1.246
PTGS2*	prostaglandin-endoperoxide	6.84E-03	↑1.448
SREBF1*	sterol regulatory element	3.57E-03	↓-1.212
TF	transferrin	6.78E-04	↓-1.677
TNFRSF11B	TNF receptor superfamily	1.16E-03	↑1.272

Supplementary Fig. 12: LXR/RXR activation pathway is predicted to be inhibited in the SGBS dataset **(A)** Predicted activation of pathways in the SGBS dataset retrieved from IPA software. Bar chart interpretation: The length of bar represents the –log(p-value), the larger the bar the more significant the p-value. Color coding is based on the z-score and takes into account the directionality of transcripts annotated to the pathway if orange, predicted activation; if blue predicted inhibition; white indicates possible activation or inhibition and gray indicates there is not enough data to make a prediction on directionality. The predictions are based literature curated in the ingenuity knowledge base available in the IPA software. The faint orange line is the significance threshold set by user, in this case 0.05 represented as –log(0.05) on the chart. Orange zig-zag line is a ratio calculated by number of transcripts in the pathway in your dataset/number of molecules in the pathway. **(B)** Transcripts annotated to the LXR/RXR signaling pathway retrieved from IPA software. NR1HR which codes for the LXRα nuclear receptor is downregulated in SULT1A1 knockout SGBS.

Supplementary Figure 13

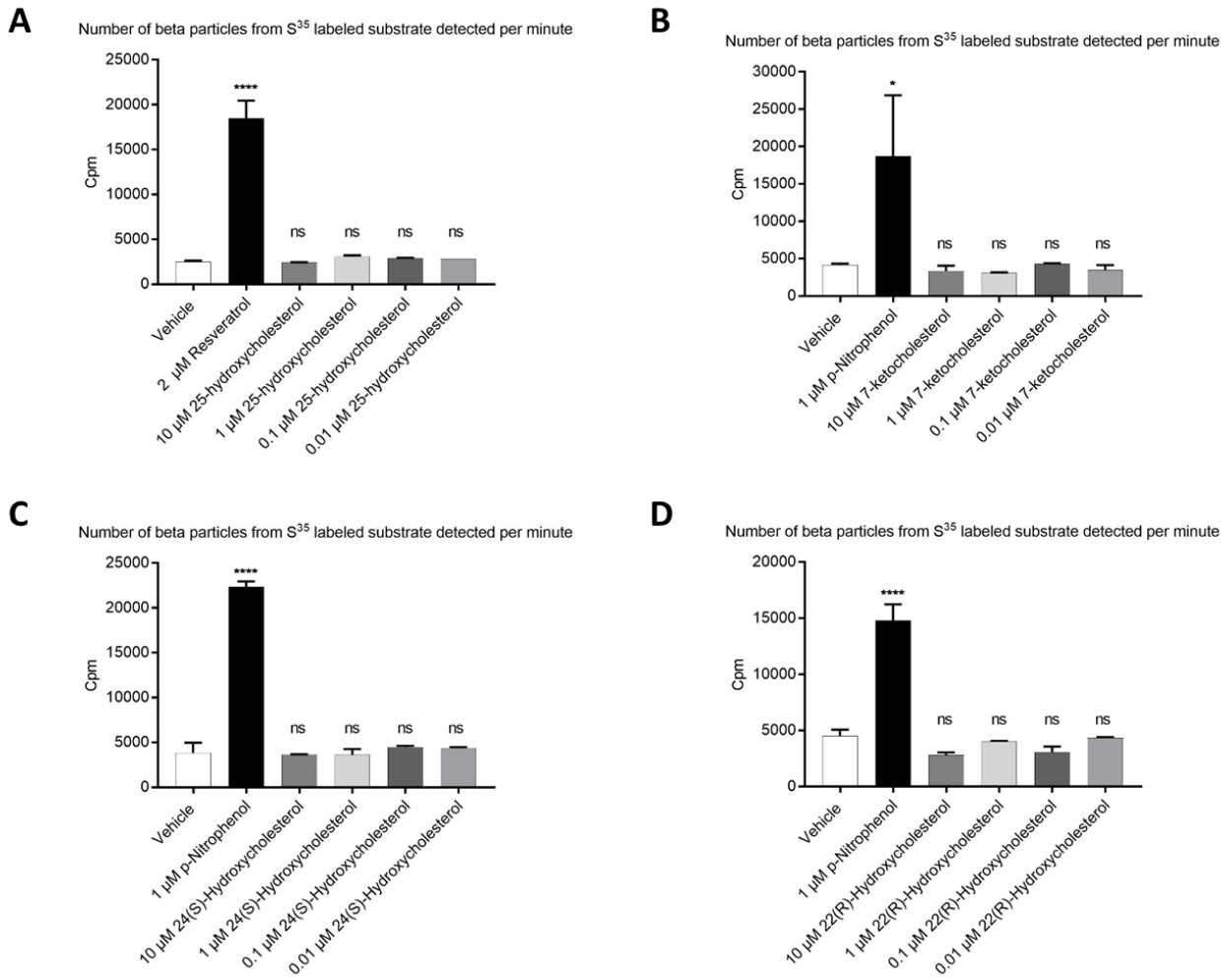

Supplementary Fig. 13: Radiochemical assay to test the affinity of oxysterols to SULT1A1. Each condition was measured in duplicates. Vehicle was the negative control and contained DMSO only. Positive control SULT1A1 substrates were 2 µM resveratrol for panel A and 1 µM p-Nitrophenol for panel B to D. For panel A to D the positive control substrates had a significant increase in counts per minute (cmp) indicating that the radiolabeled S-35 from PAPS was transferred to the substrate confirming that resveratrol and p-Nitrophenol are substrates for SULT1A1. There was no significant difference between vehicle and the oxysterol conditions. The oxysterols tested were (A) 25-hydroxycholesterol (B) 7-ketocholesterol (C) 24(S)-hydroxycholesterol and (D) 22(R)-hydroxycholesterol at 10, 1, 0.1 and 0.01 µM.

Supplementary Figure 14

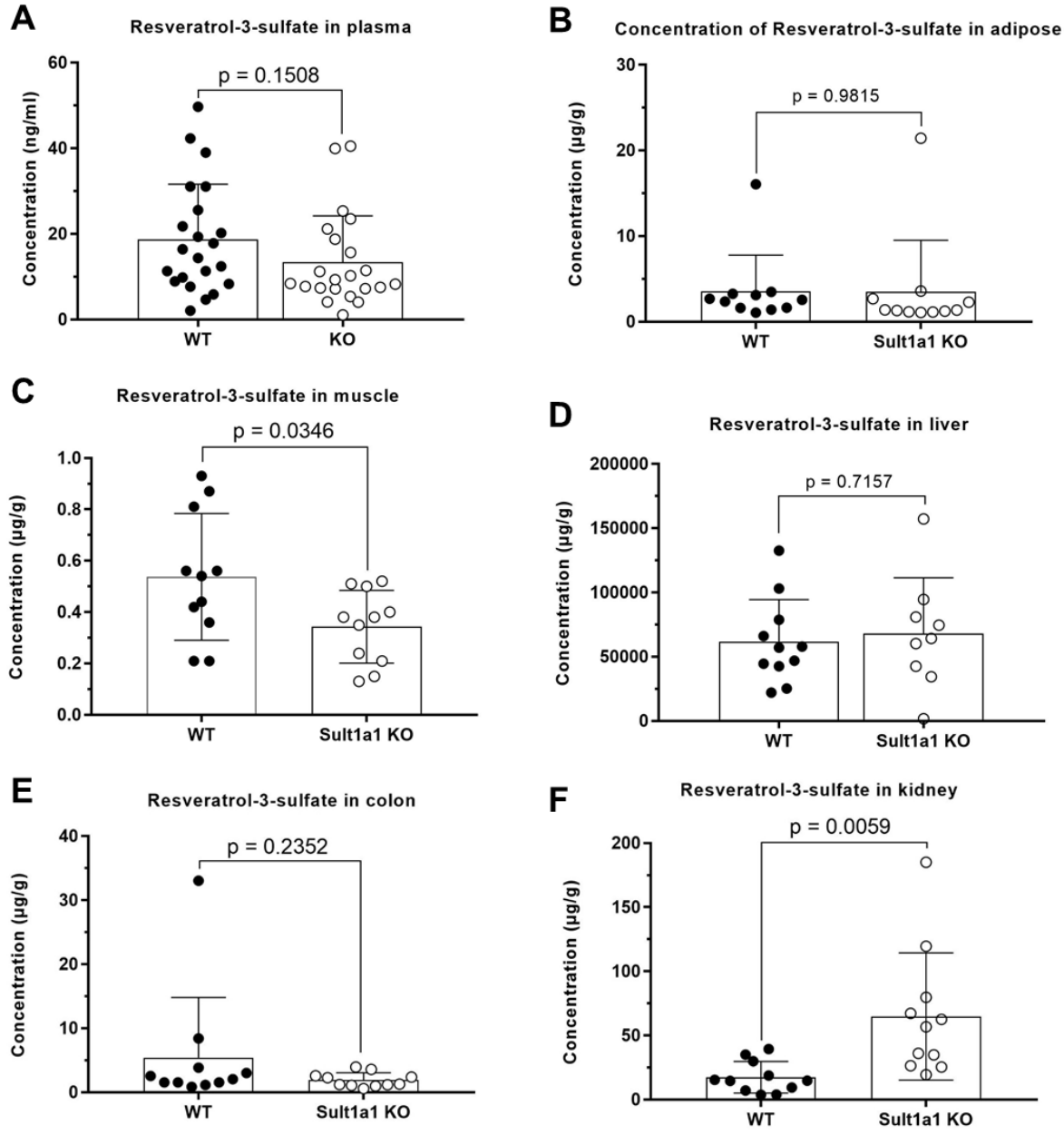

Supplementary Fig. 14: Resveratrol-3-sulfate content of (**A**) plasma (**B**) adipose (eWAT) (**C**) muscle (**D**) liver (**E**) colon and (**F**) kidney and of WT (black dots) and Sult1a1 knockout mice (white dots). Mice were dosed with 240 mg/kg body weight resveratrol. Tissues were collected 20 minutes post-dosing. n = 9-11 mice per group, plasma measured in duplicates. Data presented as mean ± standard deviation (SD); p values were calculated by using an unpaired Student's t test.

Supplementary Figure 15

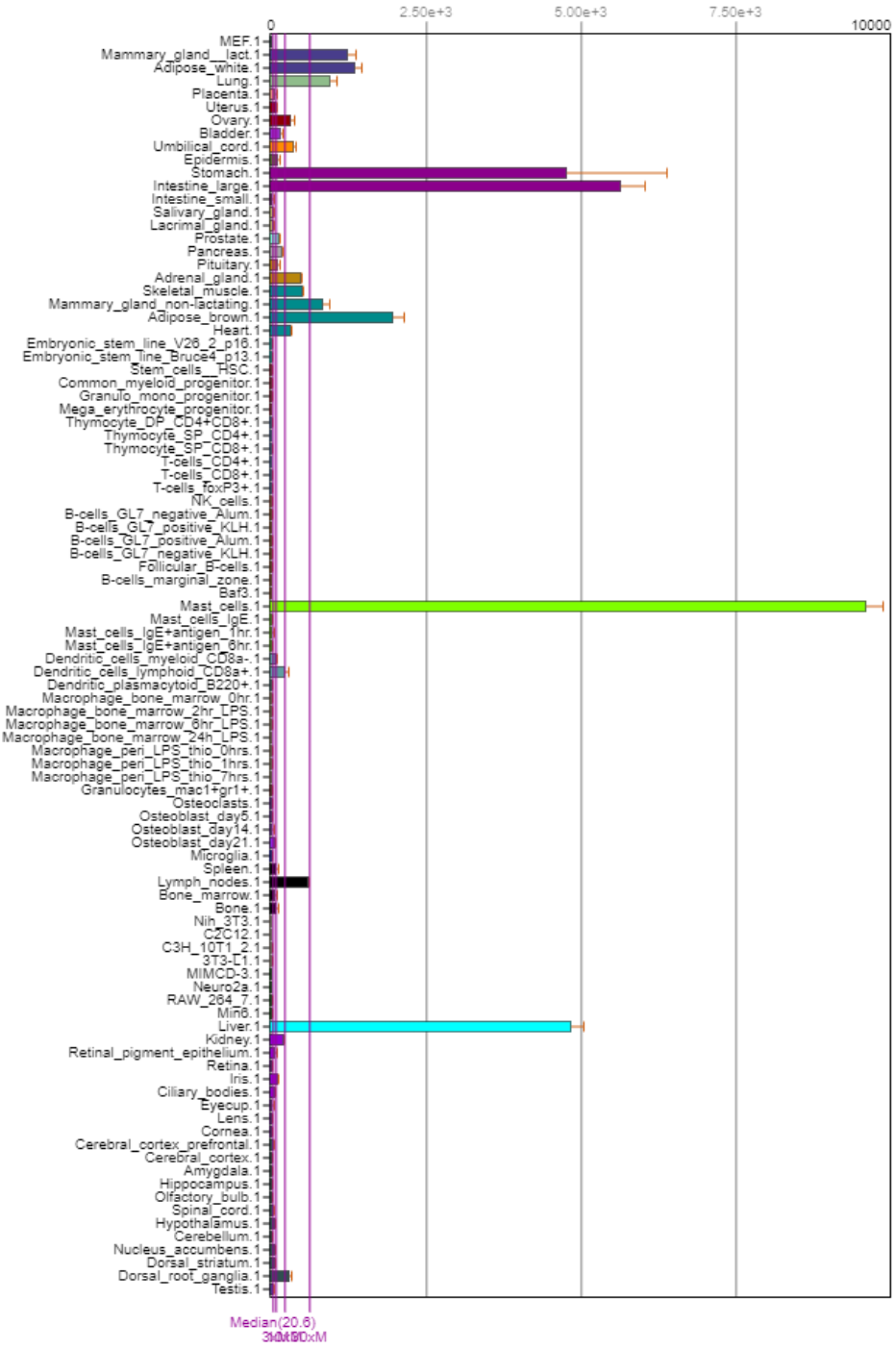

Supplementary Fig. 15: In mice, Sult1a1 is abundantly expressed mast cells, large intestine and liver. Sult1a1 expression data retrieved from BioGPS at http://biogps.org/#goto=genereport&id=20887. BioGPS is an online platform which pools data from existing gene annotation databases.

Supplementary Figure 16

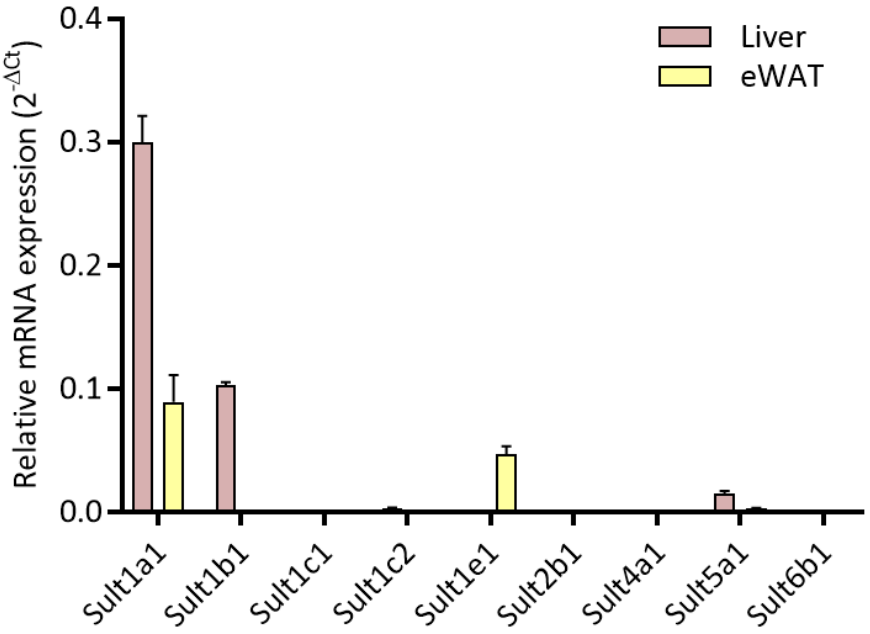

Supplementary Fig. 16: Expression of Sults in wild-type BL6J mice. Data shown as mean with SEM. mRNA expression was measured in three, 12 week old, male mouse samples (n = 3). Each sample was measured in triplicates. # indicates Sults that had a C_t value greater than 40

Supplementary Figure 17

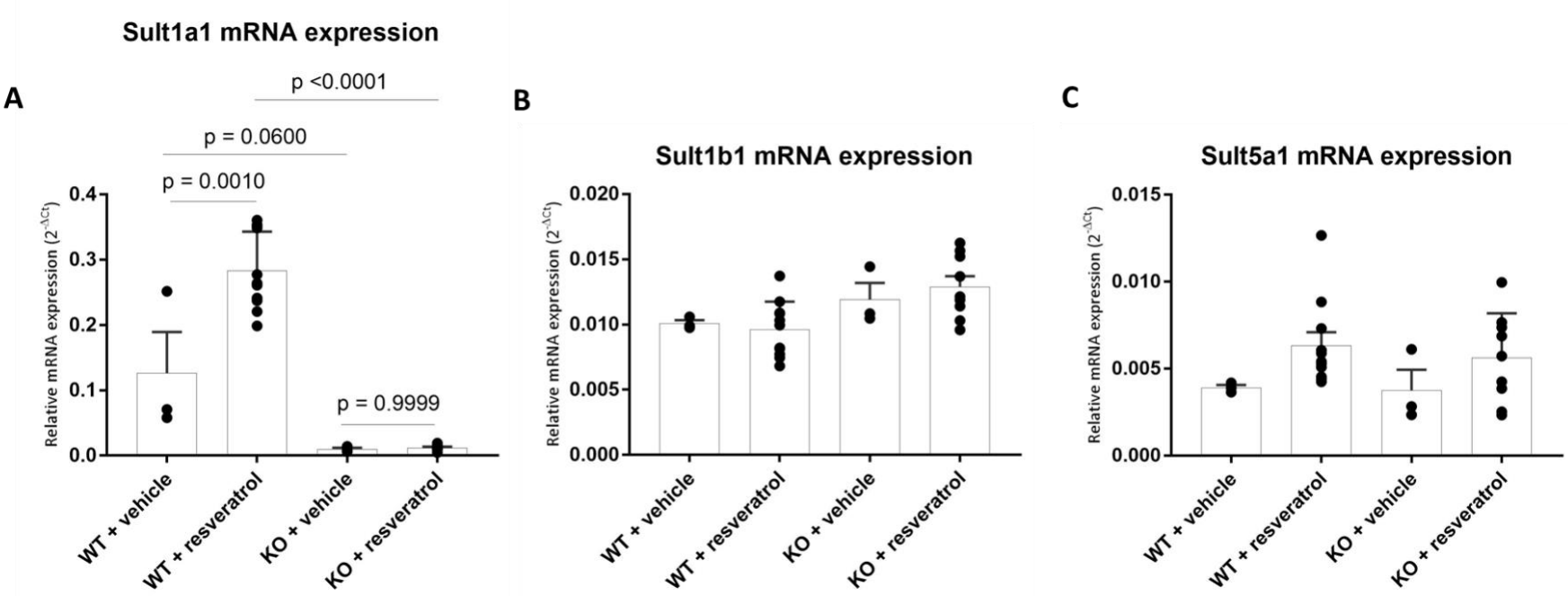

Supplementary Fig. 17: Loss of Sult1a1 is compensated by other members of the Sult family. mRNA expression of Sults in WT and Sult1a1 KO mouse liver 20 minutes post-treatment with 240 mg/kg body weight resveratrol **(A)** mRNA expression of Sult1a1 **(B)** mRNA expression of Sult1b1 **(C)** mRNA expression of Sult5a1. For vehicle treatment, n = 3 and for resveratrol treatment n = 9-11 mice per genotype.

Supplementary Table 1: Primers for genotyping Sult1a1 KO strain. Primers provided by Dr. Walter Meinl at the DIfE. The WT primer amplifies a 397 bp region of DNA spanning intron 2 and 4. The KO amplifies a 171 bp region within the neomycin cassette. The annealing temperature of both primers is 58ºC.

Gene	Primer sequence	PCR product (bp)
WT-Sult1a1 forward	CACACACTTTGGTAAGCAGGTC	397
WT-Sult1a1 reverse	GGGTTTTCTGTTAGTTGGTTGG	
KO-Sult1a1 forward	TGAATGAACTGCAGGACGAG	171
KO-Sult1a1 reverse	ATACTTTCTCGGCAGGAGCA	

Supplementary Table 2: Average litter size of WT, Sult1a1 KO and heterozygote mice

Type of cross	# of litters	# of pups	Average litter size
WT x WT	**22**	**152**	**6.9**
KO x KO	**19**	**114**	**6.0**
het x het	**62**	**585**	**9.4**

8. Extended Materials and Methods

Glycemia of the Sult1a1 KO mice strain

IPGTT and insulin measurement

IPGTT was performed on mice 16-weeks old that were fed either a HFD or a standard purified diet for 10 weeks. In parallel, blood insulin was measured during the IPGTT. Before the glucose load, blood was collected from the tail vein to measure fasting glucose and fasting insulin. After blood was collected for fasting measurements, the mice were administered a glucose bolus at a dose of 2 g/kg body weight by intraperitoneal injection. For blood glucose measurements, blood was collected at 15, 30, 60, 90 120,150 and 180 minutes after injection and measured using glucose monitor and test strips (Roche Diagnostics, Accutrend). Insulin was measured 15 and 30 minutes after the glucose bolus using 20 µl of blood. Insulin levels were measured on a BioPlex analyser (BioRad) using the Mouse Metabolic Magnetic bead panel kit (Cat # MMHMAG-44K, Millipore). The IPGTT and insulin measurement were performed after an overnight fast (16-hours) during the light period.

IPITT

IPITT was performed on mice 18-weeks old that were fed either a HFD or a standard diet for 12 weeks. The test was conducted during the light period after 4 hours fasting. Blood collected from the tail vein was used to measure fasting glucose (t = 0). Insulin was administered by intraperitoneal injection with a standardized insulin load of 1 IU/kg body weight. Blood glucose was measured at 15, 30, 60, 90 and 120 minutes post insulin injection using a blood glucose monitor and glucose test strips (Roche Diagnostics, Accutrend).

Liver histology

Median lobes were collected from mice aged 20-weeks old and immerged in embedding resin (Cryomatrix, Thermo Scientific). Freezing was performed on dry ice. Samples were stored at -80°C until sectioning on a cryostat. The samples were sectioned 10-µm thick. The frozen liver sections were stained with H&E and Oil Red O according to standardized protocols of the EPFL Histology Platform. Images were acquired using a slide scanner (VS-120, Olympus) and scale bars were added using Fiji (ImageJ) software.

SGBS transcriptomics

SGBS Cell Culture

SGBS cells were grown in filtered DMEM/F12 containing 10% FBS, 1% penicillin-streptomycin and 1% pantothenate-biotin. The SGBS cells were seeded at density of 3 x 10^5 cells in T-175 flasks and grown at 37 ˚C and 5% CO_2 until 80% confluent. At 80% confluence, adipogenic differentiation was induced by first washing the cells twice with PBS and then culturing the cells in FBS-free medium (DMEM/F12 containing 1% penicillin-streptomycin and 1% pantothenate-biotin) supplemented with a final concentration of 0.01 mg/ml transferrin, 20 nM insulin, 100 nM cortisol, 0.2 nM T_3, 25 nM dexamethasone, 250 µM IBMX and 2 µM rosiglitazone for two days.

Reverse Transfection of SGBS Cells

On day 2 the cells were prepared for reverse transfection by aspirating the media and washing the cell twice with PBS. The cells were detached from the flask by incubating the flask for 5 minutes at 37 ˚C with 2 ml of trypsin. To the flask, 8 ml of FBS containing medium (DMEM/F12 with 10% FBS, 1% penicillin-streptomycin and 1% pantothenate-biotin) was added and cells were transferred to a 50 ml Falcon tube. The cells were centrifuged at 1200 rpm for 10 minutes, the supernatant was aspirated with a pipette and the cell pellet was re-suspended with 5 ml of PBS and then the total number of cells were counted. After counting the cells, an additional 20 ml of PBS was added to the cell suspension and centrifuged at 1200 rpm for 10 minutes.

For the reverse transcription the Neon Transfection System and the Neon Transfection System 100 µl Kit were used according to the manufacturer's recommendations. Briefly, a neon tube was filled with 3 ml of Electrolytic Buffer and placed into the transfection system. The cell pellet was re-suspended in R Buffer and the SULT1A1 siRNA, SULT1A3 siRNA, and siNEG were diluted in R Buffer to 5 µM. To 2 ml of R Buffer cell suspension, 200 µl of corresponding siRNA was added. The siRNA-cell suspension mixture was pipette mixed twice and then 100 µl of the solution which contained 5 x 10^5 SGBS cells was electroporated in an electroporation pipette tip for 1 pulse at 1100 V for 20 ms. After electroporation the cells were re-seeded in one well of a 6-well plate which contained 2 ml of pre-warmed antibiotic-free FBS containing medium (DMEM/F12 with 10% FBS, and 1% pantothenate-biotin) supplemented with a final concentration of 0.01

mg/ml transferrin, 20 nM insulin, 100 nM cortisol, 0.2 nM T_3, 25 nM dexamethasone, 250 µM IBMX and 2 µM rosiglitazone. The final concentration of siRNA in each well was 25 nM.

After 24 hours, the medium was replaced with FBS-free medium (DMEM/F12 containing 1% penicillin-streptomycin and 1% pantothenate-biotin). On day 4 the differentiation medium was replaced with FBS-free medium containing a final concentration of 0.01 mg/ml transferrin, 20 nM insulin, 100 nM cortisol and 0.2 nM T_3 for 6 days. On day 10, the culture media was aspirated and samples were washed twice with 2 ml of room temperature PBS. The PBS was aspirated and then the cells were frozen at -80 ˚C until RNA extraction.

RNA Extraction and RNA Quality Measurement

The SGBS cells were lysed in 850 µl of lysis buffer with proteinase K and heated at 37 ˚C for 25 minutes in a water bath and then stored at -20 ºC until RNA extraction. RNA was extracted using Agencourt RNAdvance Tissue Kit according to the manufacturer's protocol. The Agencourt RNAdvance Tissue Kit protocol was automated with the Microlab Starplus. For the automated extraction, stock solutions of bind buffer, wash buffer, 70% ethanol and DNase were prepared and then loaded into the designated reservoirs of the Microlab Star. RNA quality was measured using the Fragment Analyzer and the Standard Sensitivity RNA Analysis Kit according to the manufacturer's instructions using 2 µl template RNA (concentration 25-500 ng/µl).

cRNA Synthesis and Hybridization

cRNA was synthesized using the Illumina TotalPrep-96 RNA Amplification Kit according to the manufacturer's protocol. 300 ng of RNA was used to produce double-stranded cDNA, followed by in vitro transcription, and cRNA labeling with biotin. 750 ng of cRNA was hybridized on an Illumina Bead Chip Array Human HT-12-v4-Bead Chip.

Quality Control and Data Analysis

Microarrays were placed and scanned in a HiScan. Differential gene expression was calculated using Partek. Differentially expressed genes were analyzed using IPA software.

Radiochemical assays to detect SULT1A1 substrates

Oxysterols (25-hydroxycholesterol (Cat # H1015), 24 (S)-hydroxycholesterol (Cat #), 7-ketocholesterol (Cat # 700015P) and 22 (R)-hydroxycholesterol (Cat # H3984), resveratrol (Cat # R5010) and p-NP (Cat # 241326) were purchased from Sigma Aldrich and diluted in DMSO prior to the assay. Each reaction contained a final concentration of 5 µM PAPS (Cat # ES019, R&D Systems), 0.09 µCi S35 radiolabelled PAPS (Cat # NEG010100UC, Perkin Elmer), 10 µg/ml recombinant SULT1A1 (provided and synthetized by Christian Chabert) and 10, 1, 0.1 or 0.01 µM oxysterols. To start the reaction, the reaction mix which contained PAPS, S35 radiolabelled PAPS recombinant SULT1A1 and oxysterol was incubated for 30 minutes at 37 ºC on a shaker set to 500 rpm. After incubation, the reaction was stopped by putting the samples on ice for 5 minutes. For precipitation of unbound PAPS, 200 µl of 0.1 M barium acetate (Cat # 1.01704.500, Merk), 200 µl of 0.3 N barium hydroxide solution (Cat # B4059, Sigma Aldrich), 0.1 M zinc sulfate (Cat # Z4750, Sigma Aldrich) was added to each reaction, mixed for 1 minute and then centrifuge for 4 minutes at 12000 rpm. 500 µl of reaction was mixed with 4 ml of liquid scintillation fluid (Perkin Elmer) for measurement in a liquid scintillation counter (Perkin Elmer).

Tissue accretion of resveratrol in WT mice

UHPLC-UV analysis of resveratrol and metabolites in WT mice

Standards and chemicals

Resveratrol, its major metabolites (resveratrol-3-O-sulfate, resveratrol-4'-O-sulfate, resveratrol-3-O-glucuronide and resveratrol-4'-O-glucuronide) and the internal standard 3-hydroxy-4'-methoxystilbene were synthesized by Dr. Robert Britton at the Leicester Cancer Research Centre. The structure and purity of the standards was confirmed by HPLC, MS and 1H-NMR. The internal standard, naringenin (> 98% purity), was purchased from Sigma. Ammonium acetate, HEPES and dimethyl sulfoxide (DMSO) were all AnalaR grade from Sigma. HPLC-grade methanol and isopropanol were obtained from Fisher Chemicals (Loughborough, UK) and water was from a Nano-Pure (Barnstead, UK) water purification system at the University of Leicester.

Preparation of the standards

All stock solution of standards were prepared by diluting samples in DMSO at 2.5 mg/mL for resveratrol and its metabolites and 1 mg/mL for the internal standard 3-Hydroxy-4'-methoxystilbene. For analysis, the stock solution were diluted in DMSO to obtain concentrations ranging from 25 to 1000 µg for resveratrol and metabolites and 0.2 mg/mL for the internal standard.

Preparation of the mobile phase

The mobile phase was prepared according to a previously published method41. The mobile phase A was composed of 5 mM ammonium acetate in distilled water (pH 6.7) with 2% isopropanol. Mobile phase B was composed of 2% isopropanol in methanol. Both mobile phases A and B were degassed by sonication for 15 minutes at room temperature prior to analysis.

Sample preparation

Adipose tissue was homogenized with 50mM HEPES buffer in a ratio of 1:3 w/v. 10 µl of the internal standard were added to the fat homogenate. 600 µl of Acetonitrile was added into 200 µL of homogenate and vortexed for 1 min. The mixture was then loaded onto a Captiva EMR-lipid 3 mL cartridge (Agilent Technologies), which was pre-conditioned with 3 mL of 20% HEPES in acetonitrile. Samples were collected by elution into a clean tube using 400µL of 20% HEPES in acetonitrile followed by 300 µL of acetonitrile. The total eluent was evaporated to dryness in a Speed Vac then the residue was reconstituted with 100µL of H2O/MeOH (v/v 1:1). 60 µl of sample was injected into the HPLC column. The standard curves for resveratrol and metabolites was prepared to cover a concentration range of 50ng/mL to 1000 ng/ml. The concentration range was based on the results of two samples collected at 10 and 30 minutes post-dosing which were measured prior to measuring the full set of samples.

Liver tissue was homogenized with 50mM HEPES buffer in a ratio of x w/v. To 50 µl of liver homogenate 25 µg/ml of naringerin, the internal standard, was added. To the sample 450 µl of 50 mM HEPES buffer and acetone (2:3, v/v) was added and then centrifuged at 13,000g, 4 °C for 10 min) 150 µL of the supernatant was removed and dried under nitrogen. The residue was reconstituted with 100µL of MeOH and H2O (1:1,v/v) and 10 µL was injected onto the column.

A 50 µl aliquot of plasma was acidified with 0.85µL of concentrated HCl and spiked with 10 µL of the internal standard, naringenin (0.5mg/mL), then extracted with 200 µL of acetone. The supernatant, obtained by

centrifuging (13,000 x g, 4°C, 10 minutes), was removed and dried under a stream of nitrogen. The residue was reconstituted in 100 µL of MeOH/H2O (1:1 v/v). 30 µL was injected onto the HPLC column, samples were measured in duplicates.

HPLC-UV settings

The HPLC system consisted of a Waters Alliance 2695 separations module. The detection wavelength was set at 325 nm and flow rate at 1 mL/min. HPLC separation was performed on a Waters Atlantis dC18 column (150 x 4.6 mm, particle size 3 µm) with an Atlantis dC18 guard column (3µm, 4.6 x 20 mm). A gradient elution was performed using mobile phase A and B as described in a previous publication41 with the following modifications starting at 18 minutes into the elution. At 18 minutes there was a gradual reduction in phase A to 5% over 4 minutes for elution of the internal standard followed by a wash with phase B for 2 minutes. After the washing step, the column was re-equilibrated for 7.5 minutes with 100% phase A to prepare the column for the next sample injection. **Supplementary Table 3** describes the elution gradient used in the HPLC analysis of resveratrol and its metabolites.

Supplementary Table 3. HPLC gradient for analysis of resveratrol and its metabolites. A% and %B represent the amount of phase A and B used, respectively.

Time (minutes)	A%	B%
0	100	0%
4	80	20%
7	80	20%
16	45	55%
18	45	55%
22	5	95%
24	5	95%
24.5	100	0%
32	100	0%

qPCR for Sults in WT mice

RNA was extracted from the liver and eWAT of BL6J mice using 30 mg and 100 mg of tissue respectively with the RNeasy Kit from Qiagen. RNA quality was measured using the Fragment Analyzer and the Standard Sensitivity RNA Analysis Kit according to the manufacturer's instructions using 2 µl template RNA. cDNA was synthesized using the High-Capacity cDNA Reverse Transcription Kit (Cat # 4368814, ThermoFisher Scientific) with 250 ng RNA according to the manufacturer's recommendations. qPCR was performed as described in main Materials and Methods section. The primer sequences used are listed in **Supplementary Table 4.**

Supplementary Table 4: Sult family enzymes primer sequences

Gene	Forward	Reverse
36B4 (housekeeper)	AGATTCGGGATATGCTGTTGG	AAAGCCTGGAAGAAGGAGGTC
Sult1a1	GAGGAAAGGTACCATTGGG	TTATCTTGGCATAGTGGGC
Sult1b1	CTAGCTGGAAATGTGGCCT	AAGTAAAGGATGCTCTTCCCT
Sult1c1	CATGTAAAGGGATGGTGGG	TTTAGGGTCCTCTTTCATGTC
Sult1c2	GATATTAAGGACCCATCTTCCCA	CGAGCTACATAAAGGAACTTACAG
Sult1e1	ATCGTGCTGCCATTCGAAGA	TGGTGTACTGTCCAGATGTTCC
Sult2b1	CGAAATGAGCTGAACAAGCA	ATGATGAGAGGTCAGCAGC
Sult4a1	CATCATCAAGGAACTGACATCTC	CCATTGTGGAGGTCAGAGG
Sult5a1	GAAGGACTTTGTGCACCAG	GTATGAATCCTGGGAAGCG
Sult6b2	ACTCCTTGGTTCCTTGGACTC	ATGGGTGCCAGATTTTGGGT

qPCR for Sult compensation in WT and Sult1a1 KO liver

RNA was extracted by adding 10 mg of liver into a FastPrep tube and 600 µl of lysis buffer. The tubes were shaken on the fast prep 2 x 1 minute at speed 6, centrifuged for 1 minute and then incubated for 25 min at 38°C until RNA extraction. RNA was extracted using Agencourt RNAdvance Tissue Kit according to the manufacturer's protocol. RNA quality was measured using the Fragment Analyzer and the Standard Sensitivity RNA Analysis Kit according to the manufacturer's instructions using 2 µl template RNA (concentration 25-500 ng/µl). cDNA was synthesized using the RT Reagent Kit (RR037B, Takara) with 250 ng of RNA according to the manufacturer's recommendations. qPCR was performed as described in main Materials and Methods section. Primers for Sult1a1, Sult1b1 and Sult5a1 are described in **Supplementary Table 4**.

9. Acknowledgements

A very heartfelt thank you to my supervisor Jörg Hager. Your unwavering positivity and enthusiasm has been such a source of support for me during my PhD. Thank you for encouraging my ideas and for supporting me in studying the Sult1a1 KO line even though it was a new experience for us both. I am grateful for your mentorship, thoughtful questions and valuable feedback. I would like to express my gratitude to my co-supervisor, Martin Klingenspor. Your advice on 'being open to your data', 'giving each experiment the consideration it deserves' and 'don't think about doing something, just do it' are pieces of advice that have helped me tremendously during my PhD and that I will take with me into the future. Jörg and Martin, thank you so very much for all your guidance.

Thank you to Société des Produits Nestlé, formerly Nestlé Research and formerly the Nestlé Institute of Health Sciences. First, thank you for the funding to pursue this PhD project. You have been my home/Nest since April 2015. Thank you for welcoming me in Switzerland as a Master's student and then for continuing to support my professional development as a PhD student.

Thank you Christian Chabert for teaching me everything I know how to do in the lab. Without your instructions and guidance, these experiments would not have been possible. Thank you for being such an excellent teacher.

Katharina Schnabl, thank you for the two weeks we spent together measuring oxygen consumption of adipose tissue. I know you spent extra time before and after the measurement to make sure everything went smoothly. Vielen Dank!

Karen Brown and Cai Hong at the University of Leicester, it was such a pleasure to work with you and to learn how to measure resveratrol and its metabolites in tissues. Thank you for all your help with the quantification and for hosting me in Leicester.

To the collaborators at Phenomin-ICS, many thanks for your help with the animal studies and a special thank you to Benoit Petit-Demouliere for all the hours we discussed the project and the best way to design the mouse experiments.

I am eternally grateful to colleagues and friends who helped me design experiments, taught me methods, helped me perform experiments or gave me materials when I needed extra: Carlès Canto, Magali Joffraud, Bertrand Bétrisey, Sonia Karaz, the Genomics Team (Sylviane Metairon, Fred Raymond, Greg Lefebvre, Lorane Texari, Alix Zollinger and Jens Stolte), Kevin Hof, Eric Aria Fernandez, Alberto Parras, Anna Weiser, Angelique Cerceillieux, Miriam Valera Alberni, Tanja Sonntag, Philipp Rhein, Ann-Kristin Hov and Christopher Wall. Thank you so very much for your willingness to help me. Thanks to Dan, Laurent, Estelle, you keep everything running so smoothly at NIHS. Also, much appreciation to the Nestlé Golf Club for little breaks from my desk and bench.

To the friends I made along the way in Freising, NIHS, EPFL and UNIL: you have made my time as a PhD student unforgettable. I truly believe that friends are the family you get to choose and I chose a rowdy, loving, caring, sweet, intelligent and talented family. Dear AK, you have been such a support for me. Thank you for always being there for me, through all the weather. I am so glad we went through this journey together, I could not have wished for a better friend to walk (/sing/dance/artistic gymnastic dance with song) through the last 4 years with.

Thank you to my surrogate European families, the Obereiners and the Hovs. Thanks for being my family while I was far away from mine and for helping me not feel so homesick. Last but not least the Springer family (Mom, Dad, Mona, Joey, Uncle Elliott and Ela): thank you for being my biggest cheerleaders.

10. Curriculum vitae

11. Eidesstattliche Erklärung

Ich erkläre an Eides statt, dass ich die bei der promotionsführenden Einrichtung

Wissenschaftszentrum Weihenstephan für Ernährung, Landnutzung und Umwelt

der TUM zur Promotionsprüfung vorgelegte Arbeit mit dem Titel:

The role of SULT1A1 in whole body metabolism and adipocyte biology

im

Lehrstuhl für Molekulare Ernährungsmedizin

unter der Anleitung und Betreuung durch: **Prof. Dr. Martin Klingenspor**
ohne sonstige Hilfe erstellt und bei der Abfassung nur die gemäß § 6 Ab. 6 und 7 Satz 2 angebotenen Hilfsmittel benutzt habe.

☒ Ich habe keine Organisation eingeschaltet, die gegen Entgelt Betreuerinnen und Betreuer für die Anfertigung von Dissertationen sucht, oder die mir obliegenden Pflichten hinsichtlich der Prüfungsleistungen für mich ganz oder teilweise erledigt.

☒ Ich habe die Dissertation in dieser oder ähnlicher Form in keinem anderen Prüfungsverfahren als Prüfungsleistung vorgelegt.

☒ Ich habe den angestrebten Doktorgrad noch nicht erworben und bin nicht in einem früheren Promotionsverfahren für den angestrebten Doktorgrad endgültig gescheitert

Die öffentlich zugängliche Promotionsordnung der TUM ist mir bekannt, insbesondere habe ich die Bedeutung von § 28 (Nichtigkeit der Promotion) und § 29 (Entzug des Doktorgrades) zur Kenntnis genommen. Ich bin mir der Konsequenzen einer falschen Eidesstattlichen Erklärung bewusst.

Mit der Aufnahme meiner personenbezogenen Daten in die Alumni-Datei bei der TUM bin ich

☒ einverstanden, ☐ nicht einverstanden.

Ort, Datum, Unterschrift